Universidad de Cantabria

*Facultad de Ciencias*

# THEORETICAL AND EXPERIMENTAL STUDY OF THE OPTICAL PHASE STATISTICS IN SEMICONDUCTOR LASERS

## (Estudio teórico y experimental de la estadística de la fase óptica en láseres de semiconductor)

Trabajo de Fin de Grado
para acceder al

**GRADO EN FÍSICA**

Autor: Iker Pascual de Zulueta Barandiaran

Director: Ángel Alberto Valle Gutiérrez

Junio - 2024

**Abstract**

This work is aimed to study a few different stochastic processes, and their most relevant statistical properties. First, the Langevin equations of one-dimensional (1D) and two-dimensional (2D) Brownian motion were solved, using numerical integration. Different integration times $\Delta t$ were used, to study the convergence of the statistical moments when reducing it. In the 1D case, the variance of the $N = 10000$ trajectories was shown to converge to a linear function of time when reducing $\Delta t$. Moreover, the probability density of the trajectories was determined to be really close to a Gaussian, after times large enough. In the 2D case, the phase of the process, $\Phi$, was studied. For that, no convergence of the variance was found when $\Delta t$ was reduced. This is because the probability density of $\Phi$ approaches a Cauchy distribution for times big enough, which was also proved with the data. The Cauchy distribution has infinite variance. Last, the experimental results of the optical phase of a semiconductor laser were analysed. This can be described by two different sets of mathematical equations. When the bias intensity of the laser is lower than the threshold $I < I_{th}$, one of them can be approximated by 1D Brownian motion, and the other by 2D Brownian motion. It was shown that the variance of the optical phase converged to a linear function of time, and the probability density of the phase noise approached a Gaussian, which gives experimental backup to the first set of equations over the second set.

**Key words:** Stochastic process, Brownian motion, optical phase, Quantum Random Number Generator

**Resumen**

El objetivo principal de este trabajo es estudiar algunos procesos estocásticos, y determinar sus propiedades estadísticas. Primero, se resolvieron las ecuaciones de Langevin del movimiento browniano unidimensional y bidimensional, mediante integración numérica. Se utilizaron diferentes tiempos de integración $\Delta t$ para estudiar la convergencia de los momentos estadísticos, con la reducción de dicho tiempo. En una dimensión, se demostró que la varianza de las $N = 10000$ trayectorias converge a una función lineal del tiempo al reducir $\Delta t$. Además, se determinó que la densidad de probabilidad de las trayectorias se aproxima a una gaussiana tras tiempos suficientemente largos. En el caso bidimensional, se estudió la fase del proceso, $\Phi$. Para dicha fase, no se encontró convergencia de la varianza al reducir $\Delta t$. Esto se debe a que la densidad de probabilidad de $\Phi$ se aproxima a una distribución de Cauchy, para tiempos suficientemente largos, lo cual también se demotró en los resultados. La distribución de Cauchy tiene una varianza infinita. Por último, se analizaron los resultados experimentales de la fase óptica de un láser de semiconductor. Esta fase se puede describir mediante dos conjuntos diferentes de ecuaciones matemáticas. Para intensidades de corriente del láser inferiores al umbral $I < I_{th}$, uno de ellos puede aproximarse al movimiento browniano 1D, y el otro al movimiento browniano 2D. Se demostró que la varianza de la fase óptica convergía a una función lineal del tiempo, y que la densidad de probabilidad del ruido en fase se aproximaba a una gaussiana. Esto respalda experimentalmente el primer conjunto de ecuaciones sobre las segundas.

**Palabras clave:** Proceso estocástico, movimiento browniano, fase óptica, generador de números aleatorios cuántico.

# Contents

**Contents** **1**

**1 Introduction** **3**
1.1 Quantum Technologies in Cryptography . . . 3
1.1.1 Quantum Key Distribution and Quantum Random Number Generators . 3
1.1.2 Optical Random Number Generators . . . 4
1.2 Motivation of this work . . . 5
1.2.1 Aims and Objectives . . . 5
1.2.2 Scientific Interest . . . 5

**2 Theoretical Background** **6**
2.1 Stochastic Processes . . . 6
2.1.1 History. Brownian Motion . . . 6
2.1.2 Formal Definition . . . 7
2.1.3 Statistical Moments . . . 7
2.1.4 Stationary and Markovian processes . . . 7
2.1.5 Continuous Stochastic Processes. The Fokker-Planck Equation . . . 8
2.1.6 Wiener Process . . . 9
2.2 Stochastic Differential Equations . . . 10
2.2.1 Definitions. White Noise . . . 10
2.2.2 Connection to the Fokker-Planck Equation . . . 10
2.2.3 Numerical Integration of SDEs . . . 11
2.3 The Semiconductor Laser . . . 12
2.3.1 General Structure of Lasers . . . 12
2.3.2 Semiconductor active medium . . . 12
2.3.3 Gain-switched lasers . . . 14
2.3.4 Semiconductor Laser Equations . . . 14

**3 Simulation of Stochastic Processes** **16**
3.1 One-Dimensional (1D) Brownian Motion . . . 16
3.1.1 Mathematical Framework . . . 16
3.1.2 Simulations . . . 16
3.2 Two-Dimensional (2D) Brownian Motion . . . 20
3.2.1 Mathematical Framework . . . 20
3.2.2 Algorithm to calculate $\Phi$ . . . 21
3.2.3 Simulations . . . 21
3.2.4 Starting Point (1,0) . . . 24

**4 Optical Phase in a Semiconductor Laser** **29**
4.1 Experimental Measurement of the Optical Phase . . . 29
4.1.1 Experimental Set Up and Method . . . 29
4.1.2 Numerical Algorithm to calculate $\varphi$ . . . 30

4.2 Results and Analysis . . . . . 31
4.2.1 Results of $\theta$ and $\varphi$ . . . . . 31
4.2.2 Statistical Moments and Distribution of $\varphi$ . . . . . 34

**5 Discussion & Conclusions** **38**
5.1 Discussion of the Experimental Results . . . . . 38
5.1.1 Semiconductor Laser Equations and Brownian Motion . . . . . 38
5.1.2 Which set of equations better describes the experimental results? . . . . 39
5.2 Conclusions . . . . . 39

**Bibliography** **41**

**Appendix A** **43**

**Appendix B** **44**

**Appendix C** **47**

# Chapter 1

# Introduction

## 1.1 Quantum Technologies in Cryptography

Cryptography is the art of protecting or enciphering information under a given code. It is essential in modern communications, since it allows sending confidential data safely, so that it can only be read by the chosen receiver. To avoid the deciphering of the message by hackers or fraudulent parties, the cryptographic system uses a series of algorithms, keys, and other mathematical tools.

To encipher a message, the sender uses a given algorithm, which the receiver can invert to recover the original information. This algorithm is usually not secret, or not very complicated, so the validity of the method relies on a given key. The algorithm uses this key, which can be a series of numbers, to encipher the message; and the receiver also needs the key to decipher it.

Symmetric-key encryption algorithms rely in a single key, which both the sender and the receiver keep secretly. Thus, if the communication of the message is compromised by an external intruder, they cannot decipher it, since they will not have access to the key. This is the case of for instance the Advanced Encryption Standard (AES) used by the US government for classified information [1].

On the other hand, asymmetric-key encryption algorithms have both a public key and a private key. This is the case of the RSA algorithm, which uses the product $P = p \times q$ of two large prime numbers as a public key. Anyone has access to the public key $P$, but the private key, which is the factorisation $(p, q)$, is kept secret. It is not feasible for a computer to factorise a big number like $P$ into primes in a short time, so the private key is safe even if $P$ is publicly known.

### 1.1.1 Quantum Key Distribution and Quantum Random Number Generators

Quantum Key Distribution (QKD) uses the inherent properties of quantum systems to generate and distribute cryptographic keys. These keys might be used in symmetric-key cryptographic algorithms, if there is an assurance that the QKD comes from the desired source [2].

QKD is part of the broader scientific field of Quantum Comunications, which consists on the transfer of information between distant parties, employing quantum states. To encode the in-

formation, quantum bits (qubits) are used. A qubit is the superposition of two eigenstates, $|0>$ and $|1>$ in a two-dimensional Hilbert space. This superposition is inherent of quantum systems, as the wave-function $\psi$ of the system can be written as $|\psi>= c_1|0> +c_2|1>$. The use of a 2D Hilbert space allows the storage of much more information than in classical binary computing, and explains the relevance of the development of quantum communications [3].

QKD is based on the exchange of quantum states, where a quantum statistical analysis provides a measure of the information leakage to a potential eavesdropper. The key advantage is that if a hacker tries to observe qubits in transit, the quantum state collapses to either $|0>$ or $|1>$. This means that the hacker will leave behind a tell-tale sign of the activity [3].

One way to create cryptographic keys is to generate a large series of random numbers. This is why Quantum Random Number Generators (QRNG) play an important role in QKD technologies. QRNGs are a particular type of hardware physical random generator, in which data are obtained from quantum events. Their main advantage is that the generated randomness is inherent to quantum mechanics, making quantum systems a perfect entropy source for random number generation. In this context, entropy is a measure of the true randomness of the method, i.e. higher entropy means that the numbers are more unpredictable. QRNGs are some of the most developed quantum technology systems, and many devices are already available in the market to consumers and companies. Most existing QRNGs are based on quantum optics because of the availability of high-quality optical components and the possibility of chip-size integration [4].

Most random numbers used in computing come from pseudorandom number generators (PRNGs), also known as deterministic random bit generators. These use deterministic algorithms to calculate a sequence of numbers, which may follow a given probability distribution and thus be considered random as a whole. The problem with these methods is that they are not random at all, and hence, anyone which knows the algorithm can reproduce the sequence of numbers.

This is why QRNGs are really important to create cryptographic keys, where its not only relevant that the sequence of numbers follows a given distribution, but also that they are actually random so that they can be kept secret. The quantum processes behind QRNGs cannot be replicated or reproduced, and therefore only the originators have access to the list of random numbers.

### 1.1.2 Optical Random Number Generators

In optical RNGs, the source of entropy is generally based on fluctuations of a light signal. These fluctuations can for instance be due to spontaneous emission noise, which makes the phase of the light fluctuate, due to spontaneous emission being random. In semiconductor lasers, for example, atoms emit light spontaneously, which creates a random noise on top of the stimulated emission characteristic to the laser. Recall stimulated emission is coherent and hence has a given constant phase. This noise is a high entropy source [5].

There is an special type of QRNG based on semiconductor lasers in which the randomness is based on spontaneous emission noise. The laser emits a pulse and then is turned down, so that spontaneous emission, which has random phase, dominates. Then, when the laser is turned up again, its stimulated emission starts again, but with a phase that is random and de-

termined by the noise. That means that the phase of this pulse and the one just before should be statistically independent. By interference of these two pulses, which might interfere either constructively or destructively due to their different phases, a random number of photons will be created. This can be measured in a photo-detector, and serve as a source of random numbers [3]. Randomness of the optical phase is at the core of this QRNG. That is why we are interested in characterising the statistics of the optical phase of the light emitted by semiconductor lasers.

## 1.2 Motivation of this work

### 1.2.1 Aims and Objectives

The main aim of this work is to understand the statistics that characterise the optical phase, and specifically the phase noise, of semiconductor laser light. Since this phase can be modelled by a stochastic process, the first objective of the work is to give a brief introduction to the mathematical field of stochastic processes. This will be done in the second chapter, where the main definitions, theorems and results of this branch are reviewed. In particular, the theory of stochastic differential equations (SDEs) will be studied.

The next objective consists on the numerical resolution of one-dimensional and two-dimensional Brownian motion. This is a stochastic process which is defined by some SDEs, which can be solved by numerical integration. The statistical moments and probability distributions of a set of solutions will be analysed, and compared to theoretical results.

Last, a set of experimental trajectories of the optical phase of a semiconductor laser will be studied. The experiment is not part of this work, but analysing them in the same way as the Brownian motion trajectories will help understand the inherent statistics of optical phase. A comparison of all the results will allow a discussion about the equations that characterise the light of semiconductor lasers.

### 1.2.2 Scientific Interest

The importance of this research work is based on the growing interest on Quantum Key Distribution and Quantum Random Number Generator technologies based on semiconductor lasers. By determining the equations that dominate the optical phase in these lasers, and the statistics of the stochastic processes that are determined by those equations, a deeper understanding on the physical basis of these technologies will be achieved. This will allow to optimise the performance and reliability of QKD systems based on lasers. Moreover, it will help ensure the generation of truly random numbers in QRNG, which are essential for cryptographic applications.

In addition to the technological and commercial interest of this work, its scientific interest is more than evident. By connecting the statistical properties of Brownian motion with those of the phase of lasers, this research provides an intriguing mathematical insight into the nature of light. It is both simple in form and complex in essence, and builds a connection between two apparently very different physical phenomena: the movement of a pollen grain in water and the emission of light by atoms. It shows that these phenomena are actually intricately bound together, by the underlying mathematics that govern them

# Chapter 2

# Theoretical Background

## 2.1 Stochastic Processes

### 2.1.1 History. Brownian Motion

In 1827, Robert Brown was investigating the fertilisation process in *Clarkia pulchella*, observing pollen grains through a microscope. He noticed that when the grains were floating over water, they moved in a very irregular way. Further analysis proved that it wasn't a biologic process, since it could be observed in chips of glass and smoke particles as well. This chaotic movement was called Brownian motion, and it was studied by many physicists in the following decades [6].

In 1905, Albert Einstein solved the mystery of Brownian motion, by attributing it to the collision of the different molecules in the fluid with the pollen grains. Einstein considered that the movement of the molecules was so complicated, that it could only be studied with a probabilistic approach. As an example, 1 dimensional Brownian motion will be studied below [7].

First let's consider a very small time interval $\tau$, such that collisions separated by $\tau$ are statistically independent. Let $x$ be the position of each particle, and $\Delta$ the change in that position after every time interval $\tau$, both real numbers. $\Delta$ is a random variable, with a normalised probability density function $\phi : \mathbb{R} \longrightarrow \mathbb{R}$, such that $\phi(\Delta) = \phi(-\Delta)$ and $\phi(\Delta) \neq 0$ only for $|\Delta| \lll 1$. If particle density in $x$ at time $t$ (number of particles per unit volume) is denoted as $f(x,t)$, then after a time $\tau$ the density will be:

$$f(x, t+\tau) = \int_{-\infty}^{\infty} f(x+\Delta, t)\phi(-\Delta)d\Delta \tag{2.1}$$

As both $\tau$ and $\Delta$ are very small quantities, Taylor expansion can be applied, to approximate the density functions as $f(x, t+\tau) \simeq f(x,t) + \tau\frac{\partial f}{\partial t}$ and $f(x+\Delta, t) \simeq f(x,t) + \Delta\frac{\partial f}{\partial x} + \frac{\Delta^2}{2}\frac{\partial^2 f}{\partial x^2}$. Introducing these into equation (2.1):

$$f(x,t) + \tau\frac{\partial f}{\partial t} = f(x,t)\int_{-\infty}^{\infty}\phi(\Delta)d\Delta + \frac{\partial f}{\partial x}\int_{-\infty}^{\infty}\Delta\phi(\Delta)d\Delta + \frac{\partial^2 f}{\partial x^2}\int_{-\infty}^{\infty}\frac{\Delta^2}{2}\phi(\Delta)d\Delta \tag{2.2}$$

The second term on the right vanishes, since $\phi$ is an even function. Defining the diffusion coefficient $D$ as the last term on the right, $D = \frac{1}{\tau}\int_{-\infty}^{\infty}\frac{\Delta^2}{2}\phi(\Delta)d\Delta$, the problem is simplified into a partial differential equation:

$$\frac{\partial f}{\partial t} = D\,\frac{\partial^2 f}{\partial x^2} \tag{2.3}$$

This is the heat or diffusion equation in 1D, with $f(x,t) = exp(-x^2/4Dt)/\sqrt{4\pi Dt}$ as fundamental solution, which is a Gaussian with mean value 0 and standard deviation $\sqrt{2Dt}$.

### 2.1.2 Formal Definition

A stochastic process is defined as a set of random variables $\{X(\theta)\}$ where $\theta$ belongs to some index set $\Theta$. In general, the random variables will be studied as functions of time, taking $\theta = t$ and $\Theta \subset \mathbb{R}$. [8]

The stochastic process $X(t)$ is characterised by its probability density function $p(x_1, t_1, x_2, t_2, ...)$, where usually $t_1 \geq t_2 \geq ....$ This is the probability distribution of measuring $X(t_1) = x_1$, $X(t_2) = x_2$ and so on. Therefore, conditional probability density functions can be defined as:

$$p(x_1, t_1, x_2, t_2, ...|y_1, \tau_1, y_2, \tau_2, ...) = \frac{p(x_1, t_1, x_2, t_2, ..., \tau_1, y_2, \tau_2, ...)}{p(y_1, \tau_1, y_2, \tau_2, ...)} \tag{2.4}$$

### 2.1.3 Statistical Moments

Given a stochastic process $X(t)$ and its probability density function $p(x, t)$, there are several definitions which can be useful:

-Mean Value: $\eta(t) = E[X(t)] := \int_{-\infty}^{\infty} xp(x, t)dx$

-Variance: $\sigma_X^2 := E[(X - E[X])^2] = E[X^2] - E[X]^2$

-Standard Deviation: $\sigma_X := \sqrt{\sigma_X^2} = \sqrt{E[X^2] - E[X]^2}$

-Autocorrelation: $R(t_1, t_2) := E[X(t_1)X(t_2)] = \int_{-\infty}^{\infty}\int_{-\infty}^{\infty} x_1 x_2 p(x_1, t_1, x_2, t_2)dx_1 dx_2$

### 2.1.4 Stationary and Markovian processes

A stochastic process is stationary if the two processes $X(t)$ and $X(t + \epsilon)$ have the same characteristics $\forall\epsilon \in \mathbb{R}$, i.e. if their probability density functions are equal:

$$p(x_1, t_1, x_2, t_2, ..., x_n, t_n) = p(x_1, t_1 + \epsilon, x_2, t_2 + \epsilon, ..., x_n, t_n + \epsilon) \quad \forall\epsilon \in \mathbb{R} \tag{2.5}$$

This means that for a single random variable $p(x, t) = p(x, t + \epsilon)$ $\forall\epsilon \in \mathbb{R}$, and hence $p(x, t) = p(x)$ $\forall t$. For two variables a new time $\tau = t_2 - t_1$ can be defined, such that $p(x_1, t_1, x_2, t_2) = p(x_1, x_2, \tau)$.

On the other hand, a stochastic process is Markovian, if the conditional probabilities only depend on the most recent past. That is, mathematically, if:

$$p(x_1, t_1, x_2, t_2, ...|y_1, \tau_1, y_2, \tau_2, ...) = p(x_1, t_1, x_2, t_2, ...|y_1, \tau_1) \tag{2.6}$$

Markovian processes have probability distributions that can be written as products of simple conditional probabilities:

$$p(x_1, t_1, x_2, t_2, ..., x_n, t_n) = p(x_1, t_1|x_2, t_2)p(x_2, t_2|x_3, t_3) \cdots p(x_{n-1}, t_{n-1}|x_n, t_n)p(x_n, t_n) \tag{2.7}$$

This is easily proved by induction on $n$. The case $n = 2$ is trivial. Let's assume it is true for $n = k - 1$, and prove it for $n = k$.

$$p(x_1, t_1, x_2, t_2, ..., x_{k-1}, t_{k-1}, x_k, t_k) = p(x_1, t_1, x_2, t_2, ..., x_{k-1}, t_{k-1}|x_k, t_k)p(x_k, t_k)$$

Since in general $P(A|C \cap D) = P(A|C|D) = P(A \cap C|D)/P(C|D)$, it is noted that

$$p(x_1, t_1|x_2, t_2, ..., x_k, t_k)p(x_2, t_2, ..., x_{k-1}, t_{k-1}|x_k, t_k) = p(x_1, t_1, x_2, t_2, ..., x_{k-1}, t_{k-1}|x_k, t_k)$$

which allows to rewrite the previous expression, taking into account that since $X(t)$ is Markovian, $p(x_1,t_1|x_2,t_2,...,x_k,t_k) = p(x_1,t_1|x_2,t_2)$:

$$p(x_1,t_1,x_2,t_2,...,x_{k-1},t_{k-1},x_k,t_k) = p(x_1,t_1|x_2,t_2)p(x_2,t_2,...,x_{k-1},t_{k-1}|x_k,t_k)p(x_k,t_k)$$

By the definition of conditional probabilities, the product of the last two terms on the right is equal to $p(x_2,t_2,...,x_k,t_k)$, which is the case $n = k-1$, and hence by the induction hypothesis allows the discussed factorisation:

$$p(x_1,t_1,x_2,t_2,...,x_k,t_k) = p(x_1,t_1|x_2,t_2)p(x_2,t_2|x_3,t_3)\cdots p(x_{k-1},t_{k-1}|x_k,t_k)p(x_k,t_k)$$

From this result, it is also relevant to write down the Chapman-Kolmogorov equation, which is trivial from the case $n = 3$:

$$p(x_1,t_1|x_3,t_3) = \int p(x_1,t_1|x_2,t_2)p(x_2,t_2|x_3,t_3)dx_2 \tag{2.8}$$

### 2.1.5 Continuous Stochastic Processes. The Fokker-Planck Equation

A stochastic process is continuous, if $X(t)$ is always a continuous function of time, for any possible process. It can be proved that a Markovian stochastic process is continuous if the following condition is met [7]:

$$\forall \epsilon > 0 \ \lim_{\Delta t \to 0} \frac{1}{\Delta t} \int_{||\vec{x}-\vec{z}||>\epsilon} p(\vec{x}, t+\Delta t|\vec{z},t)d\vec{x} = 0 \tag{2.9}$$

Considering now the 1 dimensional case, if the process satisfies the following two conditions:

$$\lim_{\Delta t \to 0} \frac{1}{\Delta t} \int_{|x-z|>\epsilon} dx\,(x-z)p(x,t+\Delta t|z,t) = A(z,t) + O(\epsilon) \tag{2.10}$$

$$\lim_{\Delta t \to 0} \frac{1}{\Delta t} \int_{|x-z|>\epsilon} dx\,(x-z)^2 p(x,t+\Delta t|z,t) = B(z,t) + O(\epsilon) \tag{2.11}$$

then the Chapman-Kolmogorov equation (2.8) can be written as [7]:

$$\frac{\partial p(z,t|y,t')}{\partial t} = -\frac{\partial}{\partial z}(A(z,t)p(z,t|y,t')) + \frac{1}{2}\frac{\partial^2}{\partial z^2}(B(z,t)p(z,t|y,t')) \tag{2.12}$$

which is the Fokker-Planck equation in 1D. The coefficients $A$ (drift coefficient) and $B$ (diffusion coefficient) are characteristic to each continuous stochastic process, and every process can be defined by its Fokker-Planck equation with those two coefficients. Let's assume now the initial condition is $p(z,t|y,t) = \delta(z-y)$. Assuming the derivatives $\partial A/\partial z \lll \partial p/\partial z$ and $\partial^2 B/\partial z^2 \lll \partial^2 p/\partial z^2$ the equation can be approximated as:

$$\frac{\partial p(z,t|y,t')}{\partial t} = -A(y,t)\frac{\partial p(z,t|y,t')}{\partial z} + \frac{1}{2}B(y,t)\frac{\partial^2 p(z,t|y,t')}{\partial z^2}$$

which has a solution $p(z,t+\Delta t|y,t)$ in the time $t+\Delta t$ which defines a Gaussian variable $y(t+\Delta t)$ with mean $y(t) + A(y,t)\Delta t$ and variance $B\Delta t$:

$$p(z,t+\Delta t|y,t) = \frac{1}{\sqrt{2\pi B\Delta t}} \exp\left(-\frac{(z-y-A(y,t)\Delta t)^2}{2B\Delta t}\right)$$

This variable $y(t+\Delta t)$ can therefore be written as a function of its variance and mean values, taking a general Gaussian variable $\eta(t) \sim \mathcal{N}(0,\sqrt{B})$:

$$y(t+\Delta t) = y(t) + A(y,t)\Delta t + \eta(t)\Delta t^{1/2} \tag{2.13}$$

This result explains how the system's mean $y + A(y,t)\Delta t$ changes with 'velocity' $A(y,t)$ (being $A(y,t)\Delta t$ the drift) and its variance is $B(y,t)\Delta t$ which defines the diffusion term.

### 2.1.6 Wiener Process

A Wiener process $W(t)$ is the solution to the Fokker-Planck equation when the drift coefficient $A = 0$ and the diffusion coefficient $B = 1$. If the initial condition of the process is $W(t_0) = \omega_0$, then the probability of the process is conditional $p(\omega, t|\omega_0, t_0)$, and satisfies the Fokker-Planck equation:

$$\frac{\partial}{\partial t}p(\omega, t|\omega_0, t_0) \;=\; \frac{1}{2}\frac{\partial^2}{\partial \omega^2}p(\omega, t|\omega_0, t_0) \tag{2.14}$$

The initial condition $W(t_0) = \omega_0$ may also be written as $p(\omega, t_0, \omega_0, t_0) = \delta(\omega - \omega_0)$. Let's now define a characteristic function $\phi(s, t) = E[e^{isW}]$, which is the same as the Fourier Transform of the probability density of $W$:

$$\phi(s, t) = E[e^{isW}] = \int_{-\infty}^{\infty} e^{is\omega}p(\omega, t|\omega_0, t_0)d\omega$$

Therefore, $p(\omega, t|\omega_0, t_0)$ will be the inverse F.T. of $\phi(s, t)$:

$$p(\omega, t|\omega_0, t_0) = \frac{1}{2\pi}\int_{-\infty}^{\infty} e^{-is\omega}\phi(s, t)ds$$

Introducing this into equation (2.14):

$$\int_{-\infty}^{\infty} e^{-is\omega}\frac{\partial \phi}{\partial t}ds = \frac{1}{2}(-is)^2\int_{-\infty}^{\infty} e^{-is\omega}\phi ds \;\Rightarrow\; \frac{\partial \phi}{\partial t} + \frac{s^2}{2}\phi = 0$$

This equation is easily integrated separating the variables:

$$\int_{\phi(s,t_0)}^{\phi(s,t)} \frac{d\phi}{\phi} = -\int_{t_0}^{t} \frac{s^2}{2}dt \;\Rightarrow\; \phi(s, t) = \phi(s, t_0)e^{-\frac{s^2}{2}(t-t_0)}$$

To calculate the initial value $\phi(s, t_0)$, the initial condition must be taken into account:

$$\phi(s, t_0) = \int_{-\infty}^{\infty} e^{is\omega}p(\omega, t_0|\omega_0, t_0)d\omega = \int_{-\infty}^{\infty} e^{is\omega}\delta(\omega - \omega_0)d\omega = e^{is\omega_0} \;\Rightarrow\; \phi(s, t) = e^{is\omega_0 - \frac{s^2}{2}(t-t_0)}$$

Finally, since $\phi(s, t)$ is the F.T. of the probability density, $p$ will be the inverse F.T., which can be calculated as:

$$p(\omega, t|\omega_0, t_0) = \frac{1}{\sqrt{2\pi(t - t_0)}}e^{-\frac{(\omega-\omega_0)^2}{2(t-t_0)}} \tag{2.15}$$

Note that the solution of the 1 dimensional diffusion equation (2.3) can also be obtained by this method of the characteristic function. Thus, the probability density of the Wiener process $W(t)$, which has been derived in (2.15), shows that $W$ is a Gaussian variable with mean value $\omega_0$ and variance $(t - t_0)$. The process $W(t)$ is characterised by a Fokker-Planck equation, and therefore, it is a continuous Markovian process. This means that:

$$p(\omega_n, t_n, ..., \omega_0, t_0) = \prod_{i=0}^{n-1} p(\omega_{i+1}, t_{i+1}|\omega_i, t_i)p(\omega_0, t_0) = \prod_{i=0}^{n-1} \frac{e^{-\frac{\Delta W_i^2}{2\Delta t_i}}}{\sqrt{2\pi(\Delta t_i)}}p(\omega_0, t_0) \tag{2.16}$$

where the differences in $W$ and $t$ are defined as $\Delta W_i := \omega_{i+1} - \omega_i$ and $\Delta t_i := t_{i+1} - t_i$. This shows that $\Delta W_i$ are independent processes, with Gaussian probability distributions of mean 0 and variance $\Delta t_i$.

## 2.2 Stochastic Differential Equations

### 2.2.1 Definitions. White Noise

Stochastic differential equations (SDEs) are differential equations in which some terms are stochastic processes $\xi(t)$. The most simple case are the Langevin equations, which have the structure:

$$\frac{dx}{dt} = a(x,t) + b(x,t)\xi(t) \tag{2.17}$$

where $a(x,t)$ and $b(x,t)$ are known functions, and $\xi(t)$ is defined to vary very fast and irregularly, i.e. for $t \neq t'$, $\xi(t)$ and $\xi(t')$ are statistically independent. If the mean value is defined to be zero, $< \xi(t) >= 0$, and

$$< \xi(t)\xi(t') > = \ \delta(t-t') \tag{2.18}$$

then $\xi(t)$ is called white noise. This name comes from the calculus of the power spectrum. This is given by the Fourier transform of the autocorrelation [7]. For the case of a Dirac's delta autocorrelation, like in (2.18), the power spectrum is one, independent of the frequency. This means it contains all the frequencies, and hence it is "white".

Equation (2.18) also implies that $\xi(t)$ and $\xi(t')$ are statistically independent, and moreover that $\xi(t)$ has infinite variance, $< (\xi(t) - < \xi(t) >)^2 >=< \xi(t)^2 >= \delta(0) = \infty$. This is obviously a mathematical idealisation, since in reality a physical variable cannot have infinite variance. Note that a new notation is being introduced, $< \xi >= E[\xi]$ for averages over realisations, because it is the most usual notation. Both notations will be used indistinguishably from now on.

Now, assuming equation (2.17) is integrable, $u(t) = \int_0^t \xi(t')dt'$ exists, and it is a continuous function of $t$, since it is an integral and $\xi(t) \in \mathbb{R}\ \forall t$. This implies that $u(t)$ is a Markovian stochastic process. To prove this let's write:

$$u(t') = \int_0^t \xi(s)ds \ + \ \int_t^{t'} \xi(s)ds \ = \ \lim_{\epsilon \to 0} \left[ \int_0^{t-\epsilon} \xi(s)ds \right] + \int_t^{t'} \xi(s)ds$$

Take an $\epsilon > 0$. Since $\forall s \in [0, t-\epsilon]\ \forall s' \in [t, t']$, $\xi(s)$ and $\xi(s')$ are statistically independent, then $u(t-\epsilon)$ and $u(t') - u(t)$ are also independent. Therefore, by continuity $u(t)$ and $u(t') - u(t)$ are statistically independent, which proves that the stochastic process $u$ is a Markovian process.

### 2.2.2 Connection to the Fokker-Planck Equation

The stochastic process $u(t)$ from above is Markovian and continuous, and thus it is the solution of a given Fokker-Planck equation. The goal now is to calculate the drift and diffusion coefficients. For that let's write the process $u(t)$ in the form of equation (2.13), taking $u(t) = u_0$ as initial condition:

$$u(t + \Delta t) - u(t) = A(u_0, t)\Delta t + \eta(t)\Delta t^{1/2}$$

where $\eta(t) \sim \mathcal{N}(0, \sqrt{B})$. Now taking mean values, at the limit when $\Delta t$ approaches zero, the calculation of the drift coefficient $A$ is as follows:

$$A = \lim_{\Delta t \to 0} \frac{< u(t + \Delta t) - u_0 >}{\Delta t} \tag{2.19}$$

since $< \eta(t) >= 0$. Analogously, taking the mean value of $(u(t + \Delta t) - u(t))^2$, again since $< \eta(t) >= 0$ and $< \eta(t)^2 >= B$ the diffusion coefficient is derived as:

$$B = \lim_{\Delta t \to 0} \frac{< (u(t + \Delta t) - u_0)^2 >}{\Delta t} \tag{2.20}$$

Therefore, calculating now those quantities:

$$< u(t+\Delta t)-u_0 >=< \int_0^{t+\Delta t} \xi(s)ds - \int_0^t \xi(s)ds >=< \int_t^{t+\Delta t} \xi(s)ds >= \int_t^{t+\Delta t} < \xi(s) > ds = 0$$

$$< (u(t+\Delta t)-u_0)^2 >=< \int_t^{t+\Delta t}\int_t^{t+\Delta t} \xi(s)\xi(s')dsds' >=$$

$$= \int_t^{t+\Delta t}\int_t^{t+\Delta t} < \xi(s)\xi(s') > dsds' = \int_t^{t+\Delta t}\int_t^{t+\Delta t} \delta(s-s')dsds' = \int_t^{t+\Delta t} ds = \Delta t$$

The coefficients $A$ and $B$ follow then from equations (2.19) and (2.20) as $A = 0$ and $B = 1$. These coefficients characterise a Fokker-Planck equation with a solution which is, by definition, a Wiener process. Hence, the process $u(t) = \int_0^t \xi(s)ds = W(t)$, and therefore, the differential of the Wiener process is $dW(t) = W(t+dt) - W(t) = \int_t^{t+\Delta t} \xi(s)ds$:

$$dW(t) = \xi(t)dt \tag{2.21}$$

In general, following the previous reasoning, it can be proved that the stochastic differential equation (2.17) is equivalent to the Fokker-Planck equation [7]:

$$\frac{\partial p(x,t|x_0,t_0)}{\partial t} = -\frac{\partial}{\partial x}\left[a(x,t)p(x,t|x_0,t_0)\right] + \frac{1}{2}\frac{\partial^2}{\partial x^2}\left[b(x,t)^2 p(x,t|x_0,t_0)\right] \tag{2.22}$$

and hence, the stochastic process $X(t)$ must be continuous and Markovian.

### 2.2.3 Numerical Integration of SDEs

Lastly, let's study how to solve the SDE in (2.17) using a numerical algorithm, which is the method which will be followed on the next chapter of this work. Let's rewrite the general SDE:

$$\frac{dx}{dt} = a(x,t) + b(x,t)\xi(t)$$

where $\xi(t)$ is a Gaussian with mean 0 and $< \xi(t)\xi(t') > = \delta(t-t')$. Now, discretising the time variable $t$ into a set of points $\{t_i\}_{i=1,\dots,N}$ such that $t_{i+1} - t_i \equiv \Delta t_i$, the equation can be rewritten into an iterative process:

$$x(t_i + \Delta t_i) - x(t_i) = a(x(t_i), t_i)\Delta t_i + b(x(t_i), t_i)[W(t_{i+1}) - W(t_i)]$$

since $dW(t) = \xi(t)dt$ or discretely $\Delta W_i \equiv W(t_{i+1}) - W(t_i) = \xi(t_i)\Delta t_i$. Now, recalling that equation (2.16) proves $\Delta W_i$ are Gaussian with mean 0 and variance $\Delta t_i$, the previous equation can be written as follows, with $\Delta W_i = \sqrt{\Delta t_i} Z_i$ where $\{Z_i\}_i$ are independent Gaussian variables $Z_i \sim \mathcal{N}(0,1)$:

$$x^{(i+1)} = x^{(i)} + a(x^{(i)}, t_i)\Delta t + b(x^{(i)}, t_i)\sqrt{\Delta t_i} Z_i \tag{2.23}$$

rewriting $x^{(i)} := x(t_i)$. This is the final equation for a simple algorithm for solving a Langevin equation, and will be used in the following sections of this work.

## 2.3 The Semiconductor Laser

### 2.3.1 General Structure of Lasers

Lasers (Light Amplification by Stimulated Emission of Radiation) are devices that create coherent light, i.e. light with a well defined wavelength, with high intensity. Stimulated emission happens when an excited atom is hit by a photon of the correct energy, and causes the atom to emit another photon with the same wavelength, direction and phase. Any laser consists of an active medium, which is the material where the light is created, and two mirrors in both sides of it. One mirror is usually totally reflective, while the other is partially transmitting, and lets the laser light out. A general scheme of a laser from [9] is shown in Figure 2.1.

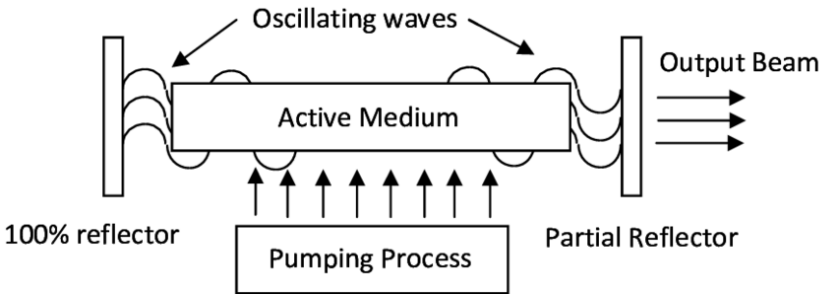


Figure 2.1: Scheme of a general laser. The stimulated radiation is produced in the active medium, and the mirrors help increase its instensity by a cascade effect [9].

The active medium needs an external source of energy, a pumping process, to emit light. The atoms in the medium get excited to higher energies by the pumping process, and as they are hit by some photons, some produce stimulated emission. At the same time this emission can be reflected in the mirrors, and stimulates other atoms to emit more light. In this manner, a cascade effect is created, which produces high intensity light with a given energy and direction. In the case of a laser in which the pumping process relies on the application of an electrical current, the minimum electrical intensity needed to activate the medium and start laser emission is called the threshold intensity $I_{th}$.

### 2.3.2 Semiconductor active medium

In semiconductor materials, the energy gap between the valence band (VB) and the conduction band (CB) is relatively small (around 1 eV). At $T = 0$K the valence band is full and the conduction band is totally empty. When temperature increases, electrons from the VB are thermically excited to the CB, and electron-hole pairs are created.

When a photon of energy similar to the band-gap strikes the material, it may induce the recombination of an electron-hole pair, and the stimulated emission of a photon. To enhance this process and create a cascade, many electron-hole pairs are needed in a small space. This is why p-n junctions are used to create lasers. Applying a negative voltage to the n region and a positive voltage to the p region (direct polarisation) the p-n junction will be full of pairs, which may then recombine [10]. This is shown in Figure 2.2:

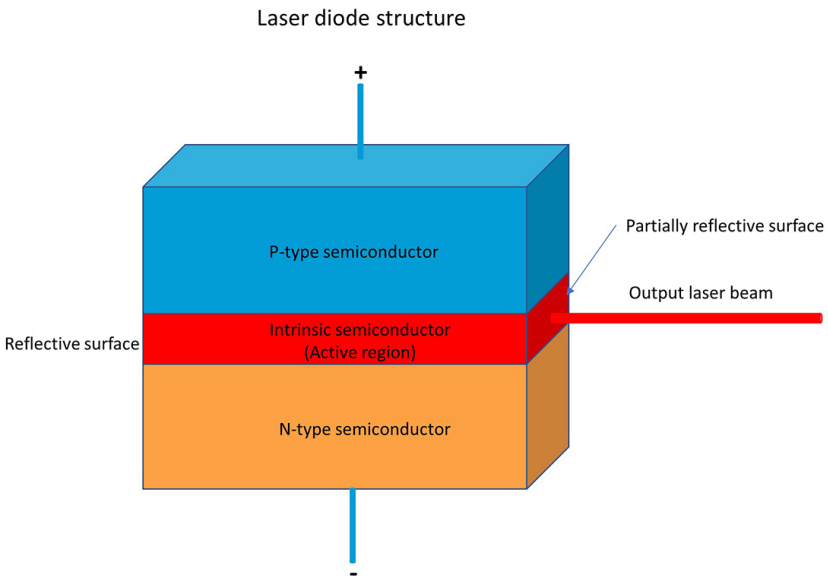


Figure 2.2: Scheme of a semiconductor laser. Direct polarisation is applied to a p-n junction to increase the number of electron-hole pairs [11].

Modern semiconductor lasers are made out of several p-n heterojunction layers, which form a heterostructure. This is specially designed to confine the charge carriers in the active medium of the laser. For this purpose, these heterostructures have semiconductors of different energy gaps. Moreover, they are such that the refractive indexes of the internal layers are larger than those of the surrounding layers, also producing a confinement of the light by total internal reflection. The energy diagram of a semiconductor heterojunction is shown in Figure 2.3.

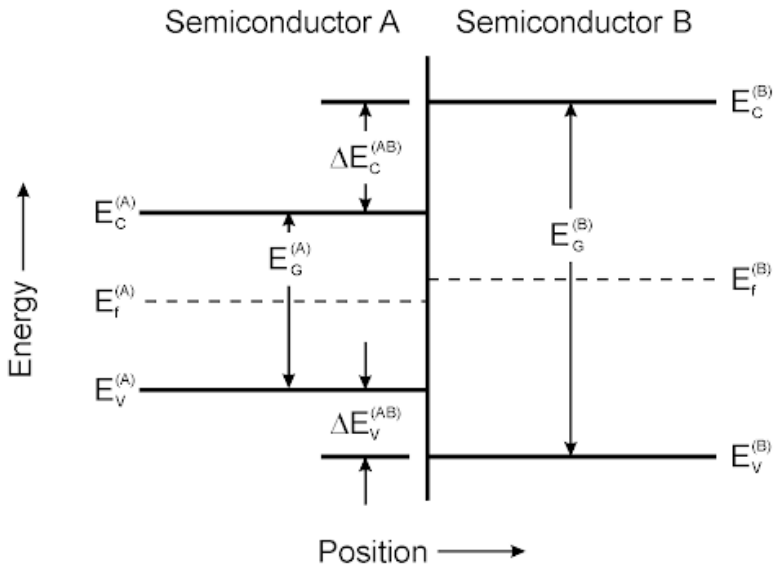


Figure 2.3: Energy diagram of a semiconductor heterojunction. The energy gap of semiconductor A is smaller than B, and the refractive index of A is larger than B. This produces the confinement of both charge carriers and light inside the structure [12].

### 2.3.3 Gain-switched lasers

Gain-switching is a technique usually employed in semiconductor-laser QRNGs, where the pumping of energy is modulated to oscillate between different intensities, so that the laser emits in short and intense pulses. When a laser receives a sudden increase in pump power, there is a delay before laser emission begins, and the active medium stores that pump energy over some time. After turning the pump power off, or lowering it under the threshold, this energy can be emitted in the form of an intense pulse. This is usually shorter than the pulse of pump power, as is exemplified in Figure 2.4 from [13].

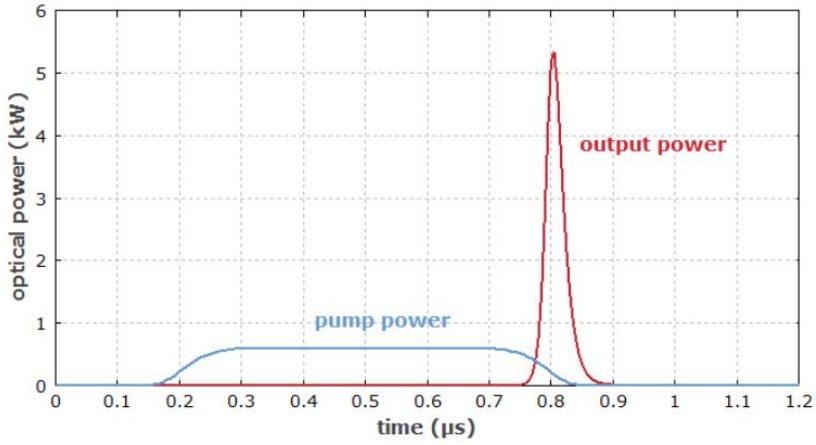


Figure 2.4: Pulses of pump power and subsequent output power in a gain switched laser [13].

### 2.3.4 Semiconductor Laser Equations

There are different sets of stochastic differential equations that are typically used to describe the light emitted by semiconductor lasers. The first one written here has been derived from first principles, for a system in equilibrium and with a constant current $I(t) \equiv I$ [14]:

$$\frac{dP}{dt} = \left[\frac{G_N(N-N_t)}{1+\epsilon P} - \frac{1}{\tau_p}\right] P + \beta B N^2 + \sqrt{2\beta B \bar{P}}\bar{N} F_P(t) \tag{2.24}$$

$$\frac{d\phi}{dt} = \frac{\alpha}{2}\left[G_N(N-N_t) - \frac{1}{\tau_P}\right] + \sqrt{\frac{\beta B}{2\bar{P}}}\bar{N} F_\phi(t) \tag{2.25}$$

$$\frac{dN}{dt} = \frac{I}{e} - (AN + BN^2 + CN^3) - \frac{G_N(N-N_t)P}{1+\epsilon P} \tag{2.26}$$

where $P(t)$ is the photon number inside the laser, $\phi(t)$ is the optical phase in the reference frame corresponding to the resonant frequency $\omega_{th}$ at the threshold current [15], and $N(t)$ is the number of carriers in the active region. The parameters appearing in the equations are the following: $G_N$ is the differential gain, $N_t$ is the carrier number at transparency, $\epsilon$ is the non-linear gain coefficient, $\tau_P$ is the photon lifetime, $\beta$ is the fraction of spontaneous emission coupled into the lasing mode, $\alpha$ is the linewidth enhancement factor, $I$ is the injected current, $e$ is the electron charge, and $A, B$ and $C$ are the non-radiative, spontaneous, and Auger recombination coefficients, respectively.

The terms $F_P(t)$ and $F_\phi(t)$ are Gaussian white noises, with $< F_i(t) >=0$ and $< F_i(t)F_j(t') >= \delta_{ij}\delta(t-t')$. Note that the current $I$ has a constant value, and variables $\bar{P}$ and $\bar{N}$ are averages over time.

In many applications, though, semiconductor lasers are used with a current $I(t)$ that changes over time. For this case, there are no rate equations derived from first principles. The usual way to act has therefore been to substitute the averages $\bar{P}$ and $\bar{N}$ in equations (2.24)-(2.26) by their corresponding variables [16]:

$$\frac{dP}{dt} = \left[\frac{G_N(N-N_t)}{1+\epsilon P} - \frac{1}{\tau_p}\right] P + \beta B N^2 + \sqrt{2\beta B P} N F_p(t) \tag{2.27}$$

$$\frac{d\Phi}{dt} = \frac{\alpha}{2}\left[G_N(N-N_t) - \frac{1}{\tau_p}\right] + \sqrt{\frac{\beta B}{2P}} N F_\phi(t) \tag{2.28}$$

$$\frac{dN}{dt} = \frac{I(t)}{e} - (AN + BN^2 + CN^3) - \frac{G_N(N-N_t)P}{1+\epsilon P} \tag{2.29}$$

where $\Phi$ is again the optical phase, written in capital to differentiate the equations. The integration of equations (2.27)-(2.28) is unstable when $I(t) < I_{th}$ due to the presence of the terms $P^{1/2}$ and $P^{-1/2}$. That is why it is interesting to write the equivalent equations, for the complex electric field $E(t) = E_1(t) + iE_2(t)$ [17]:

$$\frac{dE}{dt} = \left[\left(\frac{1}{1+\epsilon \mid E \mid^2} + i\alpha\right) G_N(N-N_t) - \frac{1+i\alpha}{\tau_p}\right] \frac{E}{2} + \sqrt{\frac{\beta B}{2}} N \xi(t) \tag{2.30}$$

$$\frac{dN}{dt} = \frac{I(t)}{e} - (AN + BN^2 + CN^3) - \frac{G_N(N-N_t) \mid E \mid^2}{1+\epsilon \mid E \mid^2} \tag{2.31}$$

where $P(t) = \mid E \mid^2 = E_1^2 + E_2^2$, $\Phi(t) = \arctan(E_2/E_1)$, and $\xi(t) = \xi_1(t) + i\xi_2(t)$ is a complex Gaussian white noise with zero average and correlation $< \xi(t)\xi^*(t') >= 2\delta(t-t')$. These equations can be integrated to find $\Phi$ with no numerical instabilities [17].

The statistical properties of $\Phi$ and $\phi$ can be approximated by two-dimensional and one-dimensional Brownian motion, respectively, when $I < I_{th}$. In this case the noise terms in equation (2.28) and (2.25) dominate over the corresponding deterministic terms [17]. This occurs because when the current is below the threshold value, $P$ and $\bar{P}$ are very small, and thus the terms $\sqrt{\beta B/2P}$ and $\sqrt{\beta B/2\bar{P}}$ are very large. Then $\Phi$, which is obtained from equation (2.28) or (2.30), can be obtained from the approximation of (2.30): $dE_i/dt = \sqrt{\beta B/2} N \xi_i(t)$. This means that the real and imaginary part of the electric field follow a two-dimensional Brownian motion in the complex plane $(E_1, E_2)$. On the other hand, $\phi$, obtained from equation (2.25), is approximately described by $d\phi/dt = \sqrt{\beta B/2\bar{P}} \bar{N} F_\phi(t) = \text{constant} \cdot F_\phi(t)$, which is the equation of one-dimensional Brownian motion.

# Chapter 3

# Simulation of Stochastic Processes

## 3.1 One-Dimensional (1D) Brownian Motion

### 3.1.1 Mathematical Framework

In the first section of the previous chapter, Brownian motion was studied, using a function $f(x,t)$ as the particle density at every point $x$. This particle density can be interpreted as a probability density function $p(x,t) \propto f(x,t)$, which hence follows the same equation (2.3) as $f$. This is a Fokker-Planck equation of the form in (2.22):

$$\frac{\partial p}{\partial t} = -\frac{\partial}{\partial x}\left[a(x,t)\right] + \frac{1}{2}\frac{\partial^2}{\partial x^2}\left[b(x,t)^2 p\right]$$

taking $a(x,t) \equiv 0$ and $b(x,t) \equiv \sqrt{D}$, and therefore its equivalent Langevin equation is:

$$\frac{dx}{dt} = \sqrt{2D}\xi(t) \tag{3.1}$$

where $\xi(t)$ is a Gaussian white noise. Following result (2.23) from the previous chapter, this SDE can be solved numerically by the algorithm:

$$x^{(i+1)} = x^{(i)} + \sqrt{2D\Delta t}Z_i \tag{3.2}$$

where $Z_i \sim \mathcal{N}(0,1)$. This algorithm was applied to solve Brownian motion for trajectories starting at $x^{(0)} = 0$ and $t_0 = 0$, and running up to a final time $t_f = 1$. The diffusion coefficient was set to $D = 1$, all variables considered being dimensionless. The algorithm was developed to use an integrating time of $\Delta t = t_{i+1} - t_i \sim 10^{-5}$, which was varied for different purposes. Since this is very small, only the values calculated every writing time $\Delta T = 10^{-3}$ were saved. This process was repeated $N$ different times. Thus, the result was of $N$ different stochastic trajectories, also called realisations of the stochastic process, each defined by the values of $X$ over $t_f/\Delta t = 1000$ writing times $T_i$. The program that numerically calculates the trajectories is written in MATLAB and shown in Appendix 5.2.

### 3.1.2 Simulations

First, the algorithm was run for an integrating time of $\Delta t = 10^{-5}$ and $N = 10000$. Three of the trajectories are shown in Figure 3.1 below, as an example.

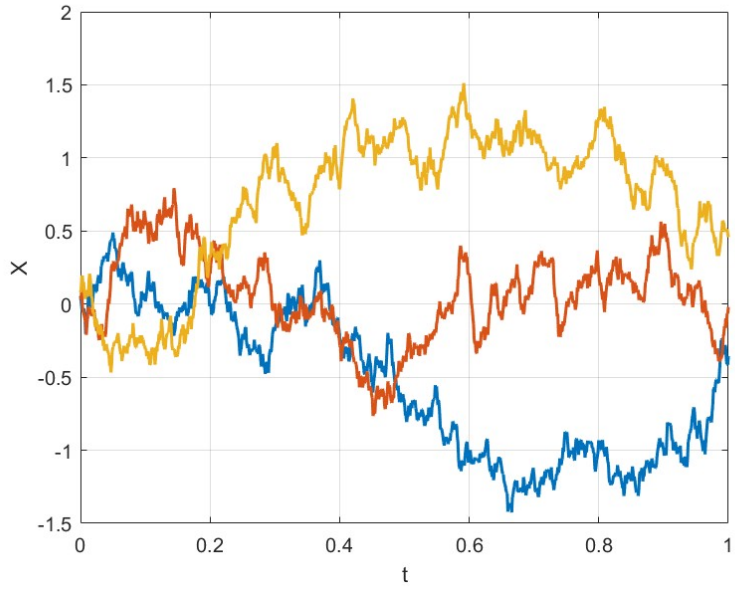


Figure 3.1: Three trajectories of 1D Brownian motion, with starting point $x^{(0)} = 0$, starting time $t_0 = 0$ and final time $t_f = 1$. The integrating time difference was $\Delta t = 10^{-5}$.

Now, taking into account all $N = 10000$ trajectories, it is of interest to calculate their mean value and standard deviation, at every writing time $T_i$. This was done and is shown in Figure 3.2.

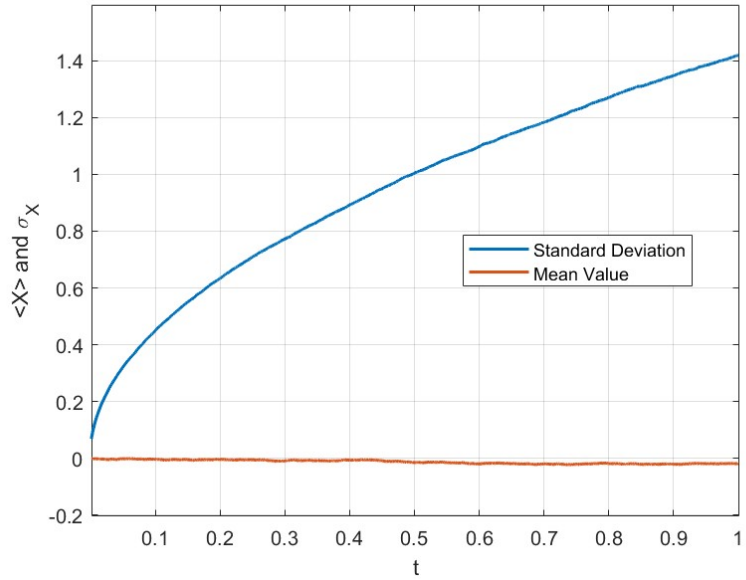


Figure 3.2: The mean value and standard deviation of all the $N = 10000$ 1D Brownian motion trajectories, with integrating time difference $\Delta t = 10^{-5}$.

Figure 3.2 shows how the mean value of all trajectories keeps very close to 0, as expected, since the probability density at any time is Gaussian with mean 0 and variance $2Dt$. The standard deviation, on the other hand, follows a function $\sqrt{2Dt}$ of time, with $D = 1$. This is also backing up the theory, since the standard deviation is defined as the square root of the variance.

Now, it is also interesting to analyse what happens to the variance when modifying the values

of $\Delta t$ and $N$. If the latter is reduced, it is easy to predict that for smaller $N$ the variance will deviate from the $2Dt$ line, since the statistical variations will have a bigger impact. This is evidenced in Figure 3.3, in which the variance was calculated for $N = 200,\ 1000$ and 10000 independent processes. The integrating time was kept constant at $\Delta t = 10^{-5}$.

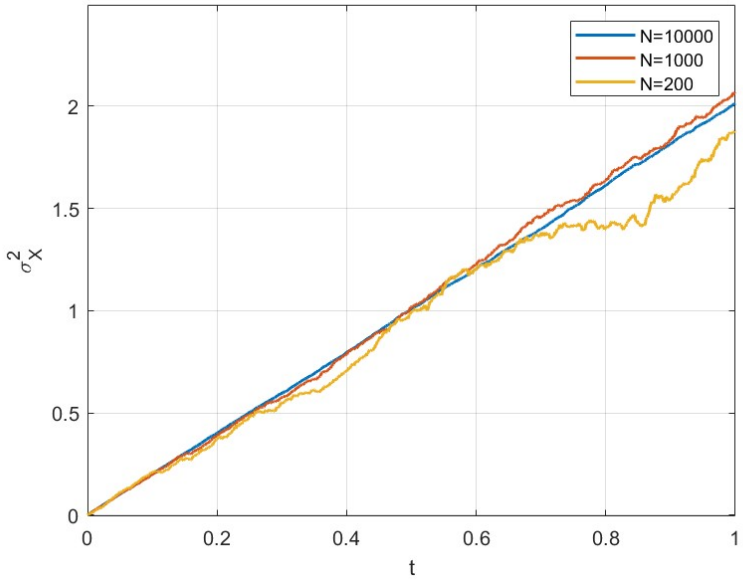


Figure 3.3: The variance of $N = 200,\ 1000$ and 10000 independent 1D Brownian motion processes, with integrating time difference $\Delta t = 10^{-5}$.

Furthermore, it is even more relevant to study how the variance converges when reducing $\Delta t$. For that, the algorithm was run three different times with $N = 10000$ and $\Delta t = 10^{-3},\ 10^{-4}$ and $10^{-5}$. The results of the computed variance are presented in Figure 3.4.

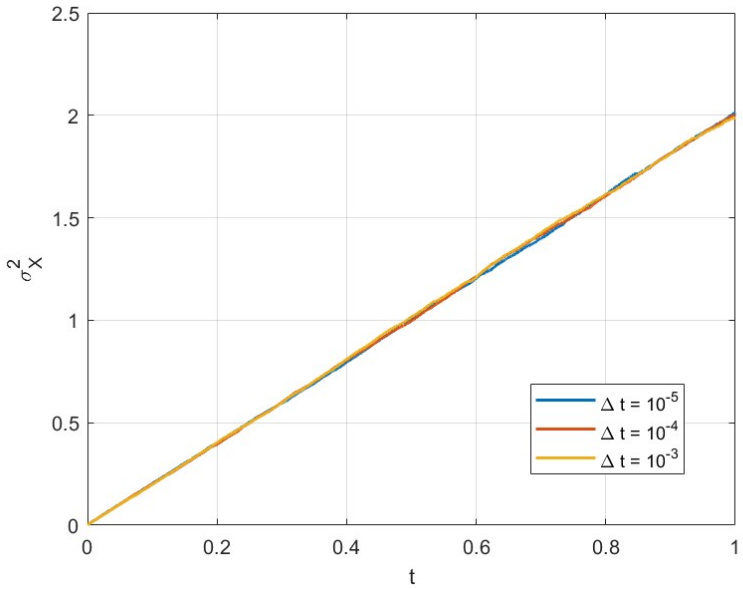


Figure 3.4: The variance of the $N = 10000$ 1D Brownian motion processes for $\Delta t = 10^{-3},\ 10^{-4}$ and $10^{-5}$.

Figure 3.4 shows how the variance converges to the theoretical line of $2Dt$ when reducing $\Delta t$, just as expected. It will be relevant to keep this in mind for the next section of this work, since

in the two-dimensional (2D) Brownian motion case, variance does not converge when reducing $\Delta t$, which is an indication of it being infinite.

As it was already pointed out several times, 1D Brownian motion has a Gaussian probability density, of mean 0 and variance $2Dt$. This means that the numerically calculated trajectories will approach a Gaussian distribution with time. For $t = 0$, the distribution is Dirac's delta, since all trajectories are at $X(t = 0) = 0$. But after enough time has passed, the distribution will start to approach a Gaussian. This can be shown by creating a histogram of the value of each trajectory at, for instance, the last time $t_f = 1$. At this point the trajectories should follow a $\mathcal{N}(0, \sqrt{2})$ distribution. This is demonstrated in Figure 3.5, comparing two histograms with $N = 1000$ (blue) and $N = 10000$ (red) with the pdf corresponding to $\mathcal{N}(0, \sqrt{2})$.

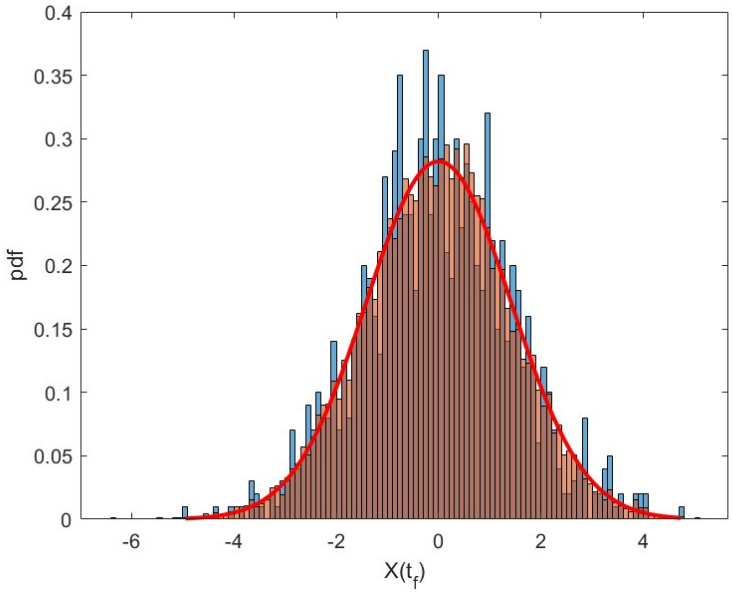


Figure 3.5: Normalised histograms of the value $X(t_f)$ of a 1D Brownian motion process for $\Delta t = 10^{-5}$ and $N = 1000$ (blue) and $N = 10000$ (red). The pdf corresponding to the $\mathcal{N}(0, \sqrt{2})$ distribution is plotted with a red line.

This clearly demonstrates how for $N = 1000$, the variable $X(t_f)$ already follows a Gaussian, and for $N = 10000$ the histogram follows the theoretical pdf closely.

## 3.2 Two-Dimensional (2D) Brownian Motion

### 3.2.1 Mathematical Framework

After the analysis of Brownian motion in one dimension, it is of interest to make the problem two-dimensional, and study what differs from the previous case. This problem is defined by the same Langevin equation (3.1), but for both variables $x_1$ and $x_2$:

$$\frac{dx_j}{dt} = \sqrt{2D}\xi_j(t) \;\; ; \;\; <\xi_j(t)>=0 \; , \; <\xi_j(t)\xi_k(t')>=\delta(t-t')\delta_{jk} \tag{3.3}$$

where $\xi_1(t)$ and $\xi_2(t)$ are Gaussian white noises, statistically independent one from the other, and $\delta_{jk}$ is Kroenecker's delta. Thus, to solve these SDEs, the same algorithm (3.2) can be used for each one of the two variables, using independent Gaussian numbers $Z_i^1$ and $Z_i^2$ for each iteration. As a result, 2D trajectories are computed, with a starting point $(x_1^{(0)}, x_2^{(0)})$.

As the two variables $x_1$ and $x_2$ are independent, and both follow the 1D Brownian motion SDE, analysing them separately will give the exact same results already discussed in section 3.1. What is novel and of relevance is to study the trajectories in polar coordinates, that is in terms of a radius $a(t)$ and an angle or phase $\Phi = \Phi(t)$.

$$\begin{cases} P(t) = a^2(t) = x_1^2 + x_2^2 \\ \Phi(t) = \arctan(x_2/x_1) \end{cases} \tag{3.4}$$

As $x_1$ and $x_2$ are independent Gaussian random variables, [17] proves that $P(t)$ is an exponential random variable, with a probability density $f(P)$ given by:

$$f(P) = \begin{cases} \frac{exp(-P/<P>)}{<P>}, \; P \geq 0 \\ 0 \qquad\quad , \; P < 0 \end{cases} \tag{3.5}$$

To calculate the mean value of $P$ is trivial from its definition, since $<P> = <x_1^2> + <x_2^2>$ $= \sigma_{x_1}^2 + <x_1>^2 + \sigma_{x_2}^2 + <x_2>^2 = 2Dt + (x_1^{(0)})^2 + 2Dt + (x_2^{(0)})^2$, so:

$$<P(t)> = \; P(0) + 4Dt \tag{3.6}$$

Regarding the phase $\Phi(t)$, [17] also shows that the stochastic differential equation that describes it is written as:

$$\frac{d\Phi}{dt} = \sqrt{\frac{2D}{P}}\xi_\Phi(t) \tag{3.7}$$

where $\xi_\Phi$ is a Gaussian white noise with $<\xi_\Phi(t)>=0$ and $<\xi_\Phi(t)\xi_\Phi(t')>=\delta(t-t')$. The variance of the phase, $\sigma_\Phi^2$, depends both on time and the inverse of the random variable $P$ [17]:

$$\sigma_\Phi^2 = 2D < 1/P > t \tag{3.8}$$

The mean value of $1/P$ is calculated by integrating it with the probability function in (3.5):

$$<1/P> = \int_0^\infty \frac{1}{P}\frac{exp(-P/<P>)}{<P>}dP = \infty \tag{3.9}$$

This proves that the variance of the phase $\sigma_\Phi^2$ diverges. This is a classical result obtained by Paul Lévy in 1940 [18]. Numerically, an infinite variance cannot be calculated. Instead, this divergence is proved by calculating the variance of a set $N$ of trajectories. For smaller integration times $\Delta t$, this variance will be higher and higher. This shows how in the limit, for an

infinitely small integration time the variance would diverge.

In fact, as F. Spitzer showed in 1958 [19], the probability density function of $\Phi$ tends, when $t \to \infty$, to a Cauchy distribution with mean value 0, defined in equation (3.10) below.

$$f(\Phi) = \frac{1}{\pi\gamma} \frac{1}{1 + \left(\frac{\Phi}{\gamma}\right)^2} \tag{3.10}$$

This distribution has an infinite variance, which is shown since the integral $\int_{-\infty}^{\infty} x^2/(1+x^2)dx$ diverges.

### 3.2.2 Algorithm to calculate $\Phi$

The phase $\Phi$ is calculated simply by determining $\arctan(x_2/x_1)$. This function, though, is defined to only take values in the interval $[-\pi/2, \pi/2]$. To maintain the continuity and unboundedness of the phase, so that it can be considered as a continuous stochastic process $\Phi(t)$ by itself, it is important to count how many times the trajectory crosses the vertical axis $x_1 = 0$. This way the phase can take any value in $\mathbb{R}$, and angles bigger than $\pi$ in module will count for how many turns the trajectory made around the origin.

For this purpose, let's describe an algorithm to calculate the phase at every integration time, developed in [17]. First, let's define two numbers: $n$ for the number of the counter-clockwise turns (cuadrant Q1 to Q2 or Q3 to Q4), and $m$ for the clockwise turns (Q2 to Q1 or Q4 to Q3). Therefore, every time the trajectory crosses the axis counterclockwise or clockwise, $n$ or $m$ are increased by 1, respectively. Naming $x_j^{(1)}$ the value of the variable $x_j$ just after the first iteration, the algorithm calculates the phase at the time $t_i$ as follows:

$$\Phi(t_i) = \Phi_i = \begin{cases} \arctan\left(\frac{x_2^{(i)}}{x_1^{(i)}}\right) + (n-m)\pi \ , & x_1^{(1)} > 0 \\ \arctan\left(\frac{x_2^{(i)}}{x_1^{(i)}}\right) + (n-m-1)\pi \ , & x_1^{(1)} < 0 \text{ and } x_2^{(1)} < 0 \\ \arctan\left(\frac{x_2^{(i)}}{x_1^{(i)}}\right) + (n-m+1)\pi \ , & x_1^{(1)} < 0 \text{ and } x_2^{(1)} > 0 \end{cases} \tag{3.11}$$

It is noted that, equation (3.11) does not take into account the diagonal crossings, between Q1 and Q3 and Q2 and Q4. To take these into account the algorithm adds or subtracts $\pi$ with 1/2 probability in those cases, considering that with a smaller integration time the trajectory was just as likely to have arrived there both clockwise or counter-clockwise. This is the main difference between using this algorithm or a predefined function in MATLAB like 'unwrap', which always minimises the phase difference in a diagonal crossing, instead of considering the 1/2 probability. The program calculates the phase for all integration times $t_i$ but only saves the data of the writing times $T_i$. The program that calculates the trajectories and implements this algorithm to determine $\Phi$ is written in MATLAB and shown in Appendix 5.2.

### 3.2.3 Simulations

The calculation of the 2D Brownian trajectories was performed as explained above, first for $(x_1^{(0)}, x_2^{(0)}) = (0, 0)$. In Figure 3.6 three independent trajectories are shown. The phase of each trajectory was calculated by the algorithm (3.11), and they are plotted in Figure 3.7 over time.

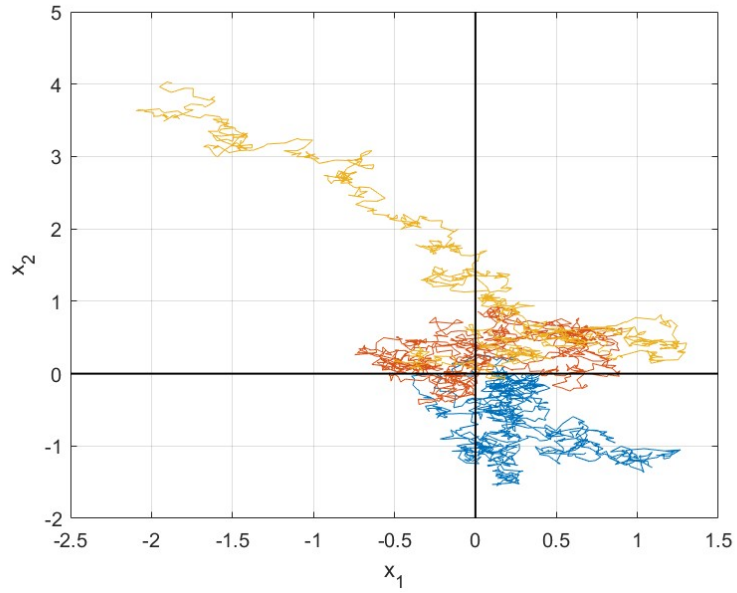


Figure 3.6: Three trajectories of 2D Brownian motion, with starting point $(x_1^{(0)}, x_2^{(0)}) = (0, 0)$, starting time $t_0 = 0$ and final time $t_f = 1$. The integrating time difference was $\Delta t = 10^{-5}$.

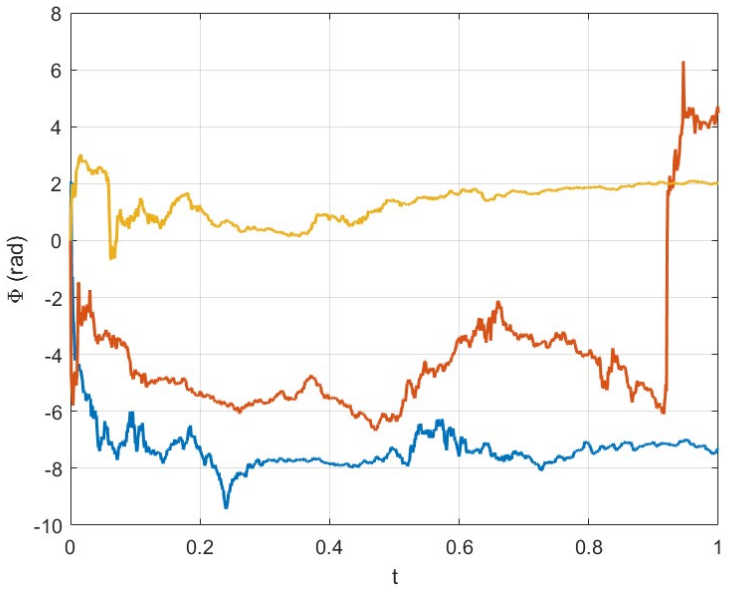


Figure 3.7: Phase $\Phi$ of the three independent 2D Brownian motion trajectories, over time $t$. $\Phi(t)$ is a stochastic process itself.

At a first look, the stochastic process $\Phi(t)$ could resemble the 1D Brownian motion trajectories in Figure 3.1. The mean value and standard deviation of $\Phi(t)$ can also be calculated, and results are in some way similar to the ones from the previous section, as shown in Figure 3.8.

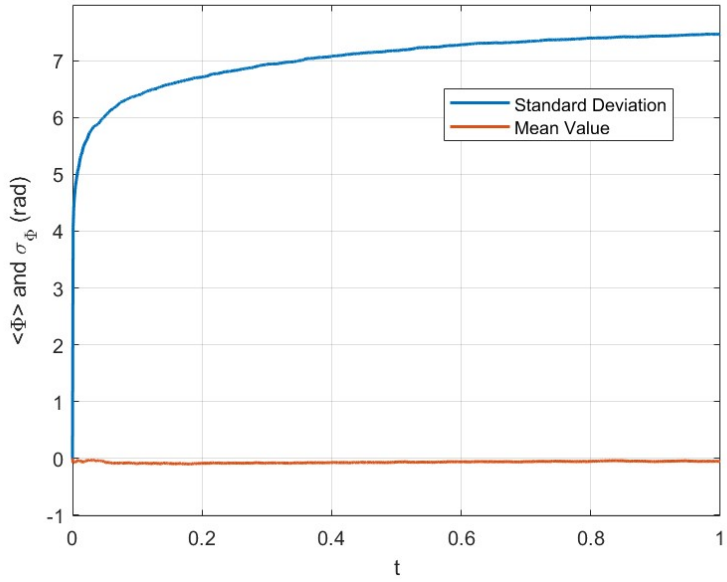


Figure 3.8: Mean value and standard deviation of the phase $\Phi$ of $N = 10000$ 2D Brownian motion trajectories.

The mean value of $\Phi$ fluctuates around 0, and the standard deviation follows something which looks like a square root, just like in the 1D Brownian motion process. However, the values of $\sigma_X$ in Figure 3.2 and $\sigma_\Phi$ in Figure 3.8 are very different. The phase $\Phi$ in Figure 3.7 changes very fast at initial times, increasing or decreasing to certain positive or negative value. Then, it can stabilise for a long period of time like in the yellow and blue trajectories in the plot. Later on, the trajectory might change abruptly again, like in the red trajectory.

This has a really simple mathematical explanation. Since the starting point is the origin (0,0), at the beginning the trajectories can move around the quadrants with very small steps, making the phase vary abruptly. Later, it is reasonable to think that the trajectory will displace from (0,0) to one of the quadrants, thus making it more difficult for $\Phi$ to change so abruptly. In the case that $(x_1, x_2)$ for any chance come back close to the origin again, like the red trajectory does, these abrupt changes can occur again.

Plotting the variance of the phase $\sigma^2_\Phi$ for $N = 10000$ trajectories, just like for 1D Brownian Motion, these abrupt changes of the phase are evident. This is done in Figure 3.9. For small times, the variance increases almost vertically. This is because as said before, $(0, 0)$ is a singular point, and when trajectories are close to it they might vary really fast. Moreover equation (3.8) shows that $\sigma^2_\Phi \propto < 1/P >$. Near $(0, 0)$ $P$ is almost 0, and $1/P$ tends to infinity.

When $P$ increases, i.e. the square of the distance to the origin increases, $1/P$ is smaller and the variance of the phase $\sigma^2_\Phi$ will increase slower. This perfectly summarizes this idea that getting closer to $(0, 0)$ involves faster variability in $\Phi$, and getting away from it means the trajectory is deep into some quadrant, with high $P$ and low phase variability. Note that here when we refer to 'the variance $\sigma^2_\Phi$' we are referring to the numerically estimated variance. The purely mathematical variance is always infinity, as also shown in Figure 3.9 by the fact that $\sigma^2_\Phi$ does not converge as $\Delta t$ decreases.

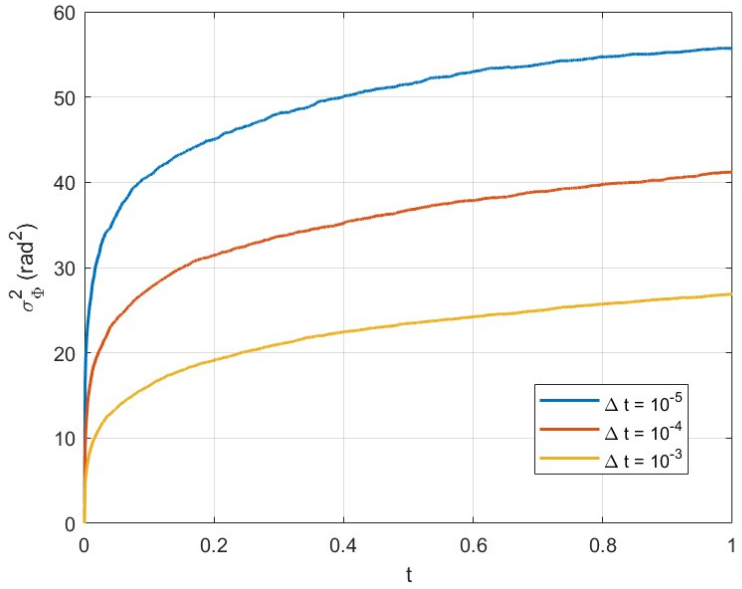


Figure 3.9: The variance of the phase $\phi$ in the $N = 10000$ 2D Brownian motion processes for $\Delta t = 10^{-3},\ 10^{-4}$ and $10^{-5}$.

### 3.2.4 Starting Point (1,0)

In the previous analysis, it was noticed how $(0, 0)$ is a singular point, since when trajectories get close to it $\Phi$ can vary really fast. To further analyse 2D Brownian motion, it seems reasonable to study processes with a starting point further away from the origin. Thus, the rapid increase of the variance for smaller times should be avoided. That is why the case $(x_1^{(0)}, x_2^{(0)}) = (1, 0)$ was studied next, which also has a starting phase $\Phi = 0$ and hence the mean $< \Phi >$ should also be zero. Three trajectories are shown in Figure 3.10 and their respective phases in Figure 3.11.

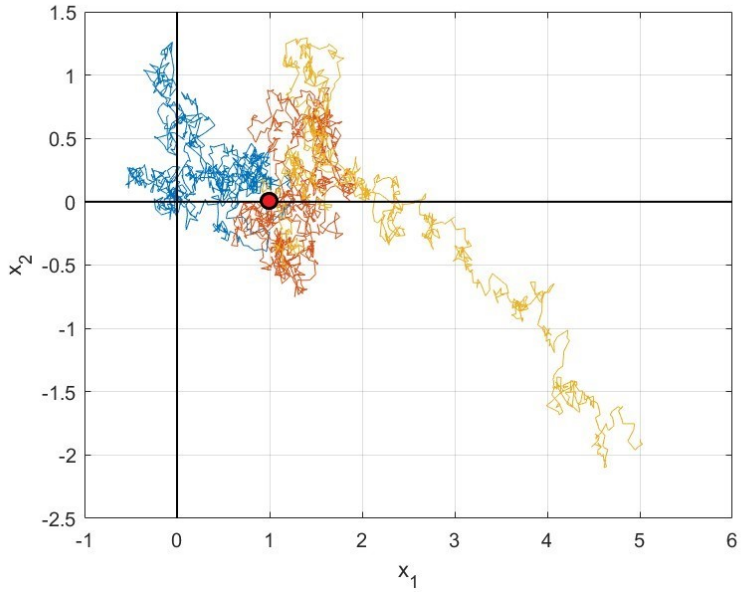


Figure 3.10: Three trajectories of 2D Brownian motion, with starting point $(x_1^{(0)}, x_2^{(0)}) = (1, 0)$, starting time $t_0 = 0$ and final time $t_f = 1$. The integrating time difference was $\Delta t = 10^{-5}$.

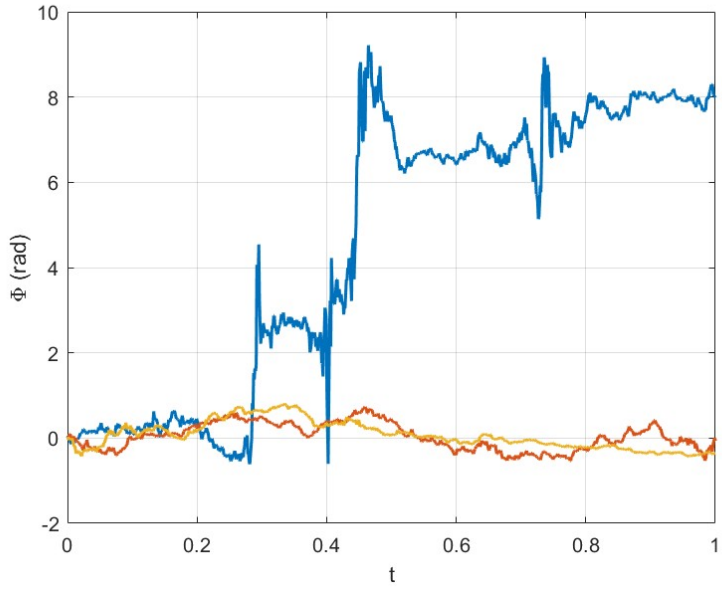


Figure 3.11: Phase $\Phi$ of the three independent 2D Brownian motion trajectories from $(x_1^{(0)}, x_2^{(0)}) = (1, 0)$.

The first result to notice is how now the phase does not abruptly change at $t = 0$, as was expected. It is interesting to analyse the variance of the phase $\sigma_\Phi^2$ over time in this case.

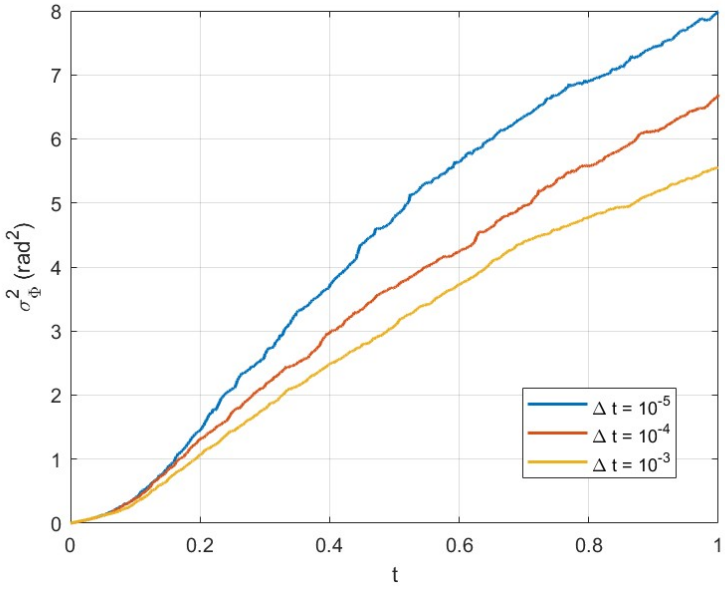


Figure 3.12: The variance of $\Phi$ for $N = 10000$ 2D Brownian motion processes, $\Delta t = 10^{-3},\ 10^{-4}$ and $10^{-5}$.

This time, the variance doesn't increase faster for small times than bigger times. Moreover, as seen before, when $\Delta t$ is reduced, the variance always increases. This is how the divergence of $\sigma_\Phi^2$ is numerically proved. In any way, $\sigma_\Phi^2$ has smaller values than in Figure 3.9 and is not a linear function of time like in 1D Brownian motion. This is once again because $\sigma_\Phi^2 \propto < 1/P >$, which is not constant since $P$ is a time-dependent random variable. To show this, in Figure 3.13 the mean value of $P$ over time for $N = 10000$ trajectories is plotted, with $\Delta t = 10^{-3}$, $10^{-4}$ and $10^{-5}$.

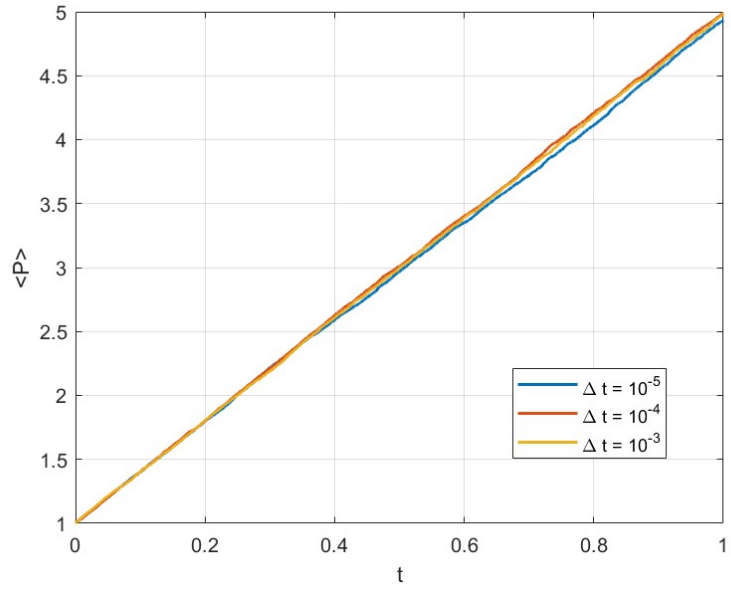


Figure 3.13: The mean of $P$ for $N = 10000$ trajectories, over time $t$.

The plot shows how equation (3.6) is fulfilled, that is $< P >= P(0) + 4Dt$. In this case $P(0) = (x_1^{(0)})^2 + (x_2^{(0)})^2 = 1$ and since $D = 1$, the slope of the line is 4. This is perfectly followed for all integration times $\Delta t$. These results show that $P$, contrary to $\Phi$, has finite moments, which do converge when $\Delta t$ is decreased. This happens because $P$ is described by an exponential distribution, as shown in (3.5). To visualise that, a histogram of all the $N = 10000$ values of $P(t_f)$ is plotted in Figure 3.14, using a logarithmic scale on the y-axis to exhibit it is exponential.

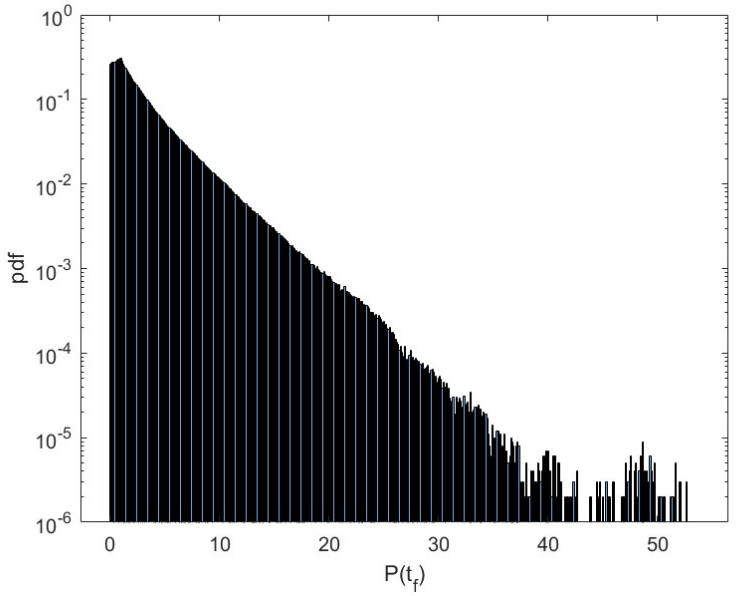


Figure 3.14: The distribution of $P(t_f)$ for $N = 10000$ trajectories. The number of trajectories is normalised and on logarithmic scale. The distribution follows a line, which shows that it is exponential.

Last, it is also insightful to study the histogram of the phase at the last time, $\Phi(t_f)$, as done with $X$ in 1D Brownian motion. This is shown in Figure 3.15, using logarithmic scale for the

number of trajectories, which are also normalised. The logarithmic scale allows to visualise better the tails of the distribution, which decrease slowly.

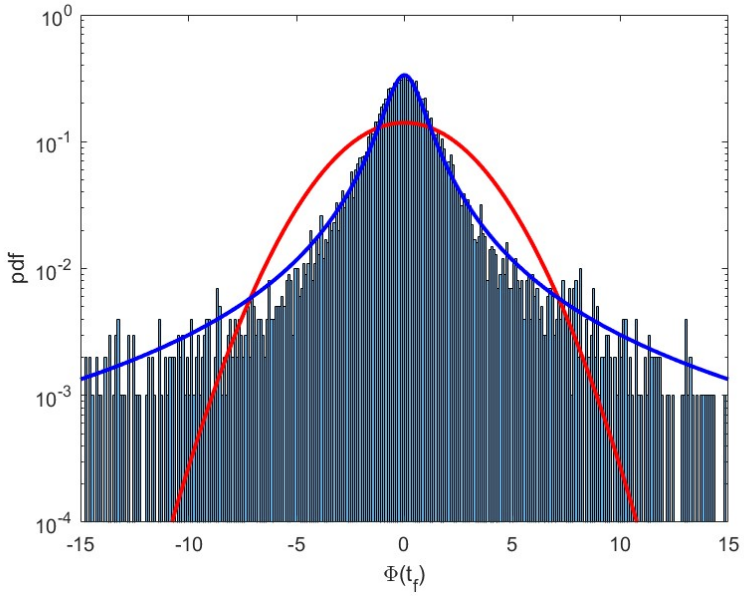


Figure 3.15: Histogram of the value $\Phi(t_f)$ of a 2D Brownian motion process for $\Delta t = 10^{-5}$ and $N = 10000$. The number of trajectories is normalised and in logarithmic scale. A Gaussian curve with the standard deviation of the data (red), and a Cauchy distribution curve (blue) are added.

The plot shows in red the Gaussian curve with the standard deviation of the data, and in blue the Cauchy distribution. The Cauchy probability approximates the data closely, specially on the tails of the distribution, where the Gaussian drops faster to zero. This explains why the Cauchy distribution's variance diverges, while the Gaussian has finite variance.

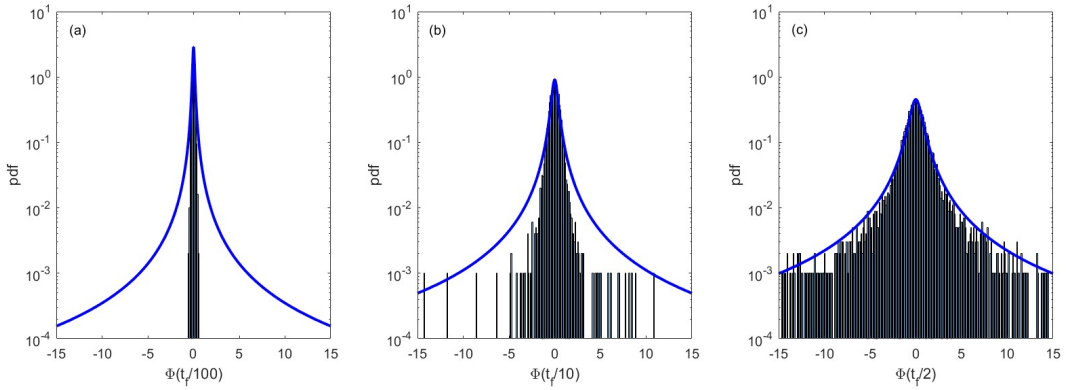


Figure 3.16: Normalised histograms of the number of trajectories with their values of $\Phi(t_f/100)$ (a), $\Phi(t_f/10)$ (b) and $\Phi(t_f/2)$ (c). Cauchy distributions are painted in blue on all of them.

In the beginning of this section it was explained how $\Phi$ would approximate the Cauchy distribution for $t \to \infty$ . But on Figure 3.15 it can be seen how $t = t_f \equiv 1$ is already a really big time in this sense, since the distribution is very close to a Cauchy. Therefore, it is insightful to analyse the distribution of $\Phi$ also at intermediate times, to try to visualise its evolution in time. It is clear that at $t = 0$ the distribution is Dirac's delta, since all trajectories start at $\Phi(0) = 0$. But with time, trajectories start to 'open up', and more and more of them will go

away from zero. In Figure 3.16 the distributions for $t = t_f/100$, $t = t_f/10$ and $t = t_f/2$ are plotted.

The results show that the distribution of trajectories approaches the Cauchy distribution very quickly in time. For $t = t_f/100 \equiv 0.01$ and $t = t_f/10 \equiv 0.1$, the distribution is already close in the center, but is quite far in the tails. For a time $t = t_f/2 \equiv 0.5$, the distribution already approximates the data closely, in the centre and the tails, just like what happens for $t = t_f \equiv 1$. This shows that $t \to \infty$, in the sense of Spitzer's theorem, in this case is already achieved for times greater than $t = 0.5$.

# Chapter 4

# Optical Phase in a Semiconductor Laser

This chapter will study the results of the experimental measurement of the optical phase in a semiconductor laser. The experiment will be briefly explained, but is not the main focus of this work, since developing it wasn't part of this Undergraduate Thesis. The goal is to study the mathematical properties of the measured data, under the stochastic process theory developed in previous chapters, to understand the relationship between the optical phase and Brownian motion processes.

## 4.1 Experimental Measurement of the Optical Phase

### 4.1.1 Experimental Set Up and Method

The experimental setup is shown in Figure 4.1. A single polarization $90^o$ optical hybrid (kylia COH24) is used to measure the phase from a single longitudinal discrete mode laser (DML), a type of semiconductor laser, with a threshold current of $I_{th} = 14.14$ mA at 25°C. The hybrid has two inputs. The light from the DML goes through an optical isolator (OI) and a polarization controller (PC), and enters one input. A tunable laser (TL) (Pure Photonics PPCL300) feeds the other input. The outputs from the hybrid go to two balanced amplified photodetectors (Thorlabs PDB480C-AC) connected to two channels of a real-time oscilloscope (Keysight DSO91204A).

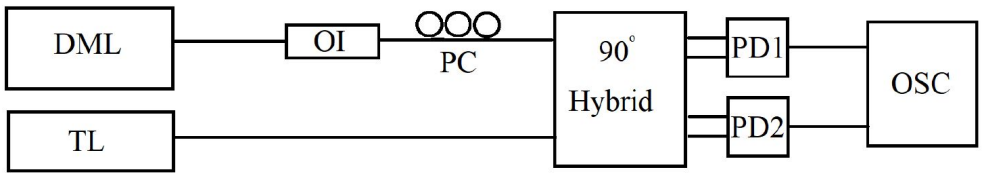


Figure 4.1: Experimental set up employed to measure the optical phase of a DML semiconductor laser.

The electrical output at photodetectors 1 and 2, PD1 and PD2, are proportional to [20]:

$$\begin{cases} PD1 = 1/\sqrt{2}S \cdot LO \cos\left[(\omega_s - \omega_{LO})t + \varphi(t)\right] \equiv E_1 \\ PD2 = 1/\sqrt{2}S \cdot LO \sin\left[(\omega_s - \omega_{LO})t + \varphi(t)\right] \equiv E_2 \end{cases} \tag{4.1}$$

where

$$S(t) = Se^{i(\omega_S t+\varphi(t))} \tag{4.2}$$

is the electric field corresponding to the DML, and

$$LO(t) = LOe^{i(\omega_{LO} t)} \tag{4.3}$$

is the electric field corresponding to the tunable laser. The linewidth of the optical spectrum of the TL is 75 kHz, much smaller than the linewidth, of the order of GHz of the DML laser close to threshold, which is the operating region on this work. That is why the phase noise of the TL is neglected. Thus the phase $\phi_S$ of the semiconductor laser is $\phi_S = \omega_S t + \varphi(t)$. $\varphi(t)$ is the phase noise of the DML laser, and is the quantity that wants to be measured and analysed. The phase $\theta(t)$ that appears in $PD1$ and $PD2$ is:

$$\theta(t) = \Delta\omega t + \varphi(t) \tag{4.4}$$

where $\Delta\omega = (\omega_S - \omega_{LO})$. Furthermore, the derivative of $\theta(t)$ over time is:

$$\frac{d\theta}{dt} = \Delta\omega + \frac{d\varphi}{dt} \tag{4.5}$$

Now, the angular frequency of the laser is $d\phi_S/dt = \omega_S + d\varphi/dt$, and its average over realisations is $< d\phi_S/dt >= \omega_S + < d\varphi/dt >$, which must be unequivocally $\omega_S$, and hence $< d\varphi/dt >= 0$. Calculating now the average over realisations of equation (4.5):

$$< \frac{d\theta}{dt} >= \Delta\omega \tag{4.6}$$

Since $d\theta/dt$ is a stationary process, averages over realisations are equal to averages over time:

$$\Delta\omega =< \frac{d\theta}{dt} > = \overline{\frac{d\theta}{dt}} := \frac{1}{T}\int_0^T \frac{d\theta}{dt} dt \tag{4.7}$$

where $T$ is an integration interval chosen to calculate all temporal averages. Therefore, once $\Delta\omega$ can be numerically calculated by (4.7), the optical phase $\varphi(t)$ can be derived from equation (4.4). Note that the parameter $\Delta\omega$ fluctuates with time, since the frequencies $\omega_S$ and $\omega_{LO}$ also fluctuate. In any laser, the inner temperature varies over time, which makes the instantaneous frequency of the laser vary. Thus, it is important to determine a time interval for which $\Delta\omega$ can be considered constant. This is the case for a time interval of $T = 1\mu$s or less, as is shown by [21].

### 4.1.2 Numerical Algorithm to calculate $\varphi$

The experimental data determined consists of three elements for each measurement: time, and $E_1$ and $E_2$, which are $PD1$ and $PD2$ in equation (4.1). The time difference between two consecutive data points is $\Delta t = t_{j+1} - t_j = 500$ps. In the measurements it is considered that the bias current applied to the DML is 14mA, just below the threshold current. The data is cut $N$ times, so that $N$ different trajectories can be considered, independent one another since the process is Markovian. $N$ is calculated so that each trajectory consists of 2000 data points, and thus, the total time of the trajectory is $T = 1\mu$s and $\Delta\omega$ can be considered constant. The data file contains data for 20 millions of times, and therefore $N = 2\cdot 10^7 \Delta t/T = 10^4$.

Running the same algorithm from subsection 3.2.2 on $E_1$ and $E_2$, $\theta(t)$ is determined, since this is the phase that appears in $PD1$ and $PD2$. To determine $\varphi(t)$, the value of $\Delta\omega$ must be

calculated, from equation (4.7) derived above. The time interval $T$ to perform the averages is chosen as the total time length of each trajectory. Now if each trajectory has $ip$ data points, $\Delta\omega$ can be numerically calculated as:

$$\Delta\omega = \frac{\overline{d\theta}}{dt} = \frac{1}{(ip-1)} \sum_{j=2}^{ip} \frac{\theta(t_{j+1}) - \theta(t_j)}{\Delta t} \tag{4.8}$$

From this, the calculation of the phase noise $\varphi(t)$ consists just on following equation (4.4):

$$\varphi(t_j) = \theta(t_j) - \Delta\omega(j \cdot \Delta t) \tag{4.9}$$

where instead of multiplying by $t_j$, $j \cdot \Delta t$ is used, so that for every trajectory it can be calculated as if $t_1 = 0$ and $t_{ip} = T$. The program that uses this algorithm to calculate the phases $\theta$ and $\varphi$ from the experimental data was written in MATLAB and is shown in Appendix 5.2.

## 4.2 Results and Analysis

### 4.2.1 Results of $\theta$ and $\varphi$

The results from an experiment like the one described in 4.1.1 will be studied. First, the algorithm from subsection 3.2.2 is applied to the data, to calculate the phase $\theta$ from $PD1$ and $PD2$. This is plotted over time for 5 different trajectories, in Figure 4.2.

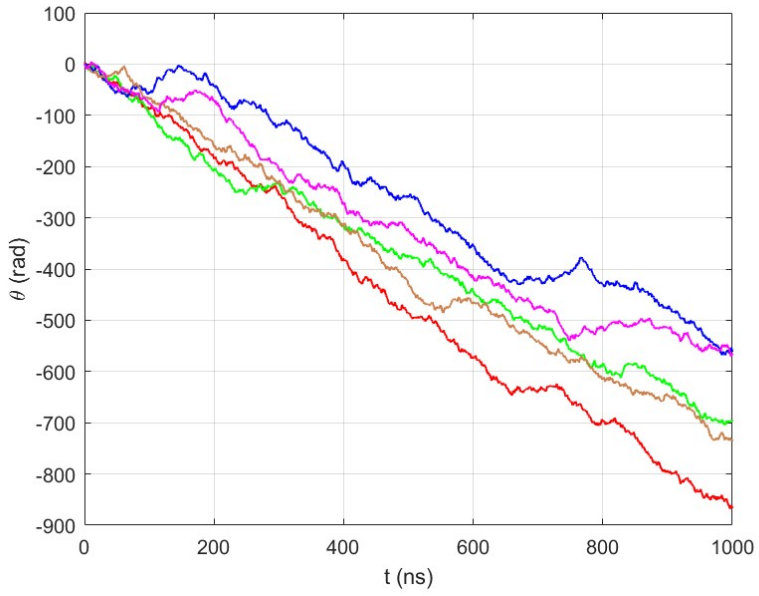


Figure 4.2: The phase $\theta$ from $PD1$ and $PD2$, over time $t$, for 5 different trajectories.

In the Figure 4.2 it is noted how $\theta$ starts at 0, and then reduces down to very negative values. This is because, as shown in equation (4.4), $\theta(t) = \Delta\omega t + \varphi(t)$, and it can be deduced $\Delta\omega$ is negative for the 5 trajectories.

In fact, in 4.1.1 it was explained how $\Delta\omega = \overline{d\theta/dt}$, but only because $d\theta/dt$ is a stationary process, i.e. its probability distribution does not depend on time. This is also evident in the experimental results. The derivative is numerically calculated as $d\theta(i)/dt = (\theta(i) - \theta(i-1))/\Delta t$, and plotted against time in Figure 4.3 for two trajectories. The time derivatives are divided by

$2\pi$, to convert from rad/s to Hz. This will be important later, when considering the instantaneous frequency $\nu$ of the laser.

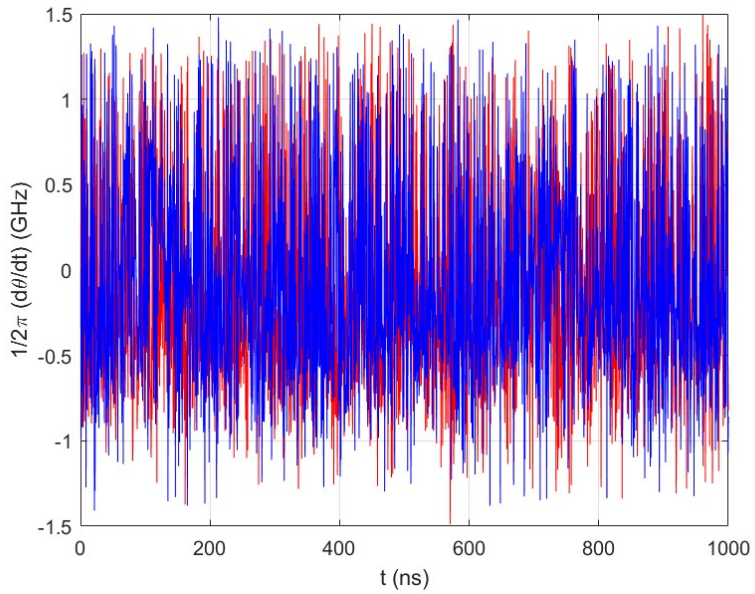


Figure 4.3: Numerical calculation of the time-derivative $1/2\pi(d\theta/dt)$, over time $t$, for 2 of the trajectories.

It can be seen how $d\theta/dt$ has the exact same evolution for different times, which is the meaning of it being stationary. Thus, the constants $\Delta\omega$ can be numerically calculated by equation (4.8). The results are shown on Figure 4.4, for 1000 different trajectories. Since, as explained in 4.1.1, the $N = 10000$ trajectories were "cut" from a single big trajectory over time, $\Delta\omega$ is plotted over time, defining times as $t_j = j * T$ where $T$ is the time-length of each trajectory.

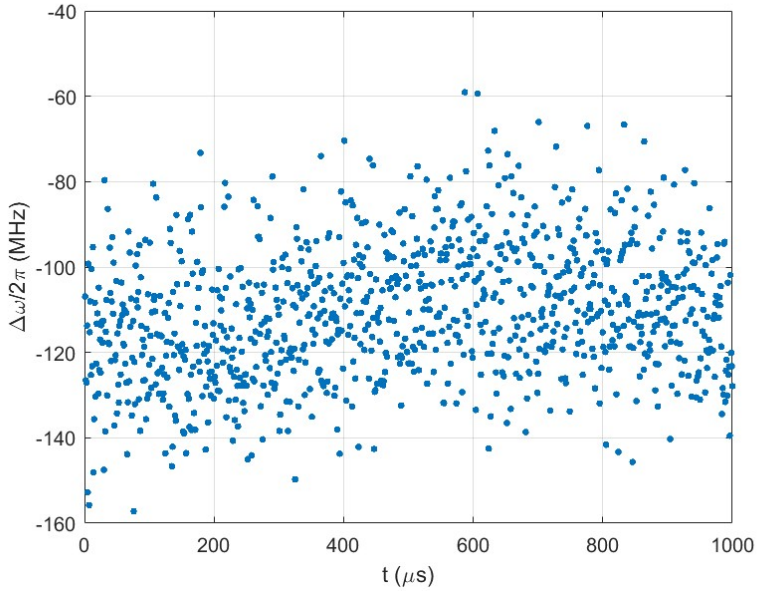


Figure 4.4: The experimental calculation of the constant $\Delta\omega$ for 1000 different trajectories, over the time $t$ characteristic to each trajectory.

Finally, since $\Delta\omega$ is known for all the $N$ trajectories, the results of $\varphi$ can be derived from

equation (4.9), as $\varphi(t) = \theta(t) - \Delta\omega t$. These are shown in Figure 4.5, for the same 5 trajectories as in Figure 4.2, over the time $t$ up to $1\mu$s; and in Figure 4.6 zooming in, for $t$ up to 125ns.

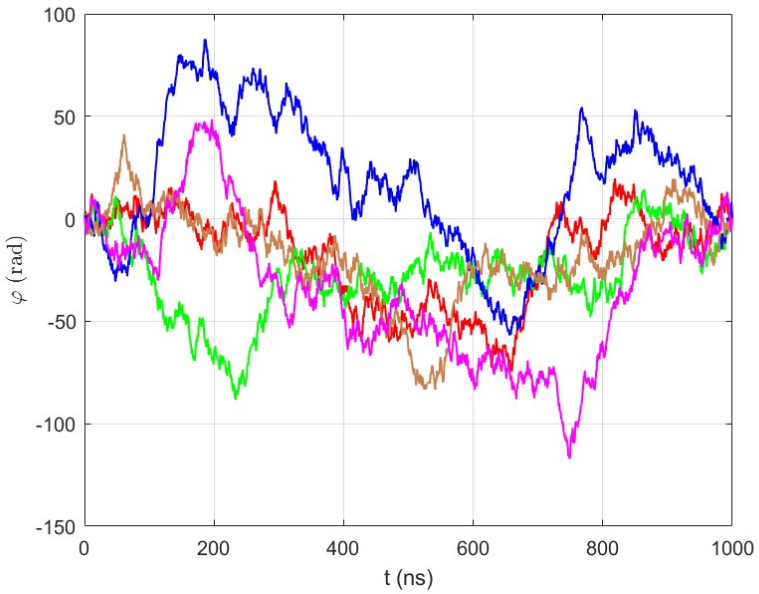


Figure 4.5: Experimental results of the phase noise $\varphi$ for the 5 different trajectories, for times $t$ from 0ns to 1000ns.

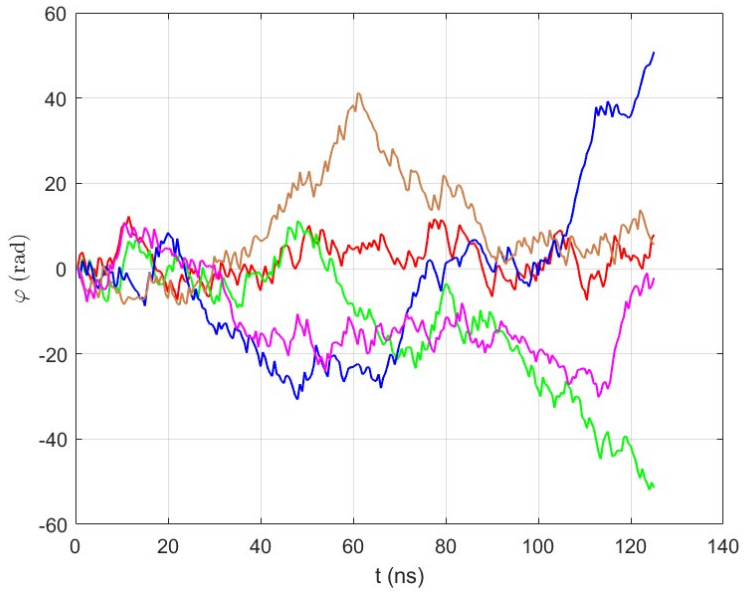


Figure 4.6: Experimental results of the phase noise $\varphi$ for the 5 different trajectories, for times $t$ from 0ns to 125ns.

Note that this is a numerical algorithm, and since time $T$ is not infinite, the results of $\Delta\omega$ are not exact, and depend strongly on the choice of $T$. In fact, as shown in the previous section $< d\varphi/dt >= 0$, which implies that:

$$\overline{\frac{d\varphi}{dt}} = \frac{1}{T}\int_0^T \frac{d\varphi}{dt}dt = 0 = \frac{1}{T}\varphi(T) \;\Rightarrow\; \varphi(T) = 0 \tag{4.10}$$

and explains why the phase noise $\varphi$ of every single trajectory in Figure 4.5 ends up at 0. This shows how $\varphi(t)$ is inevitably characterised by the choice of $T$, and that results of $\varphi(t)$ are only reliable for small times $t << T$. This is already visible analysing the results of $\varphi$ only up to a time $t = 125$ns, plotted in Figure 4.6.

It is also interesting to analyse the time derivative of $\varphi$. In Figure 4.7, the numerical time derivative $1/2\pi(d\varphi/dt)$ is plotted against time for two of the trajectories.

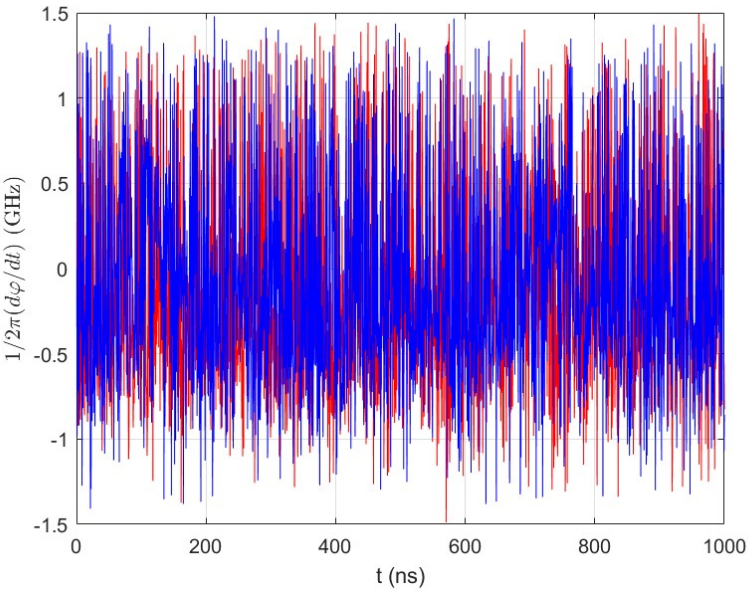


Figure 4.7: Numerical calculation of the time-derivative $1/2\pi(d\varphi/dt)$, over time $t$, for 2 of the trajectories.

The instantaneous frequency of the laser is $\nu(t) = 1/2\pi(d\phi_S/dt) = 1/2\pi(d\varphi/dt) + \omega_S/2\pi$, so the time derivative plotted in Figure 4.7 is in reality the variation between the instantaneous frequency and the optical frequency of the laser $\omega_S/2\pi$:

$$\frac{1}{2\pi}\frac{d\varphi}{dt} = \nu(t) - \frac{\omega_S}{2\pi} \tag{4.11}$$

and therefore $1/2\pi(d\varphi/dt)$ is the noise of the optical frequency. Mathematically, this noise can be described with a white noise (see section 2.3.4), since its average over time $< d\varphi/dt >$ equals 0, there is no correlation at very small time differences, and its variance is really big as can be seen in the plot. Note that the data on Figure 4.7 is limited by the bandwidth of the photodetectors, which is 1.6 GHz [20].

### 4.2.2 Statistical Moments and Distribution of $\varphi$

Given that the primary aim of this chapter is to study the optical phase noise in a semiconductor laser as a stochastic process itself, now the objective is to determine the statistical properties of the results. As done previously for Brownian motion, first let's calculate the mean value and standard deviation of $\varphi(t)$ over the $N$ trajectories. This is shown over time in Figure 4.8.

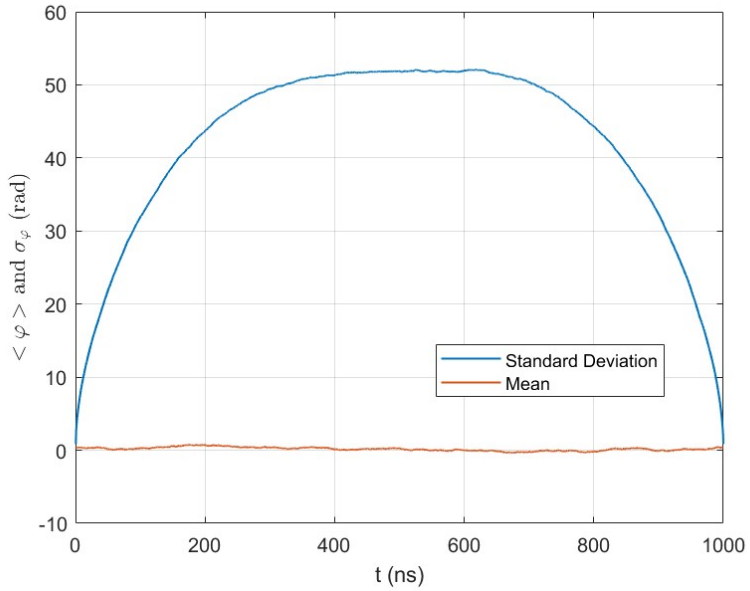


Figure 4.8: The average $< \varphi(t) >$ and standard deviation $\sigma_\varphi$ of the phase noise $\varphi$ over the $N$ realisations, versus time $t$.

As expected, the average is always really close to zero for all times. The standard deviation, on the other hand, increases at first for small times, but later starts decreasing and reaches 0 at time $t = T$. This is for the same reason why $\varphi(T) = 0$ for all trajectories, which was explained in the previous section.

As for Brownian motion, it is also relevant to study the variance of $\varphi$ for the $N = 10000$ trajectories. This is shown in Figure 4.9, versus time $t$. Since all trajectories are forced to end up at zero, $\varphi(T) = 0$, it is understandable that the variance at $t = T$ will also be zero, since there is no variation in the trajectories. But importantly, $\sigma_\varphi^2$ increases linearly with $t$ when $t << T$, a typical feature of 1D Brownian motion.

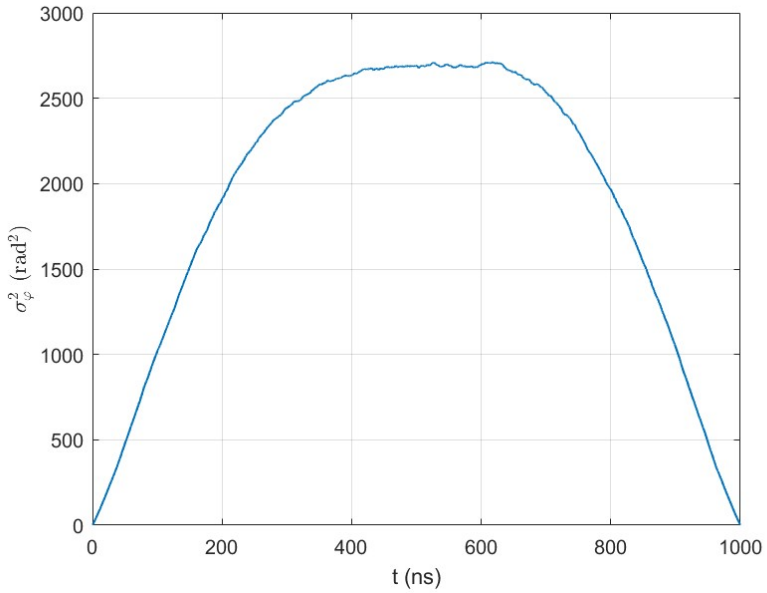


Figure 4.9: The variance $\sigma_\varphi^2$ of the phase noise $\varphi$ over the $N$ realisations, versus time $t$.

The plots prove that the choice of $T$ totally determines the resulting calculation of $\varphi$. To show this dependence between the results and the choice of the time-interval $T$, it is insightful to plot the variance over time for different values of $T$. To do this, the whole calculation of $\theta$ and $\varphi$ must be changed, since the initial list of results must be cut in trajectories of a different length $T_i$. This was done, but the same number of a total $N = 10000$ trajectories was kept, since this is considered high enough to calculate statistical moments. The results are plotted in Figure 4.10, over one time interval for $T = 1000$, 500, 200 and 100 ns.

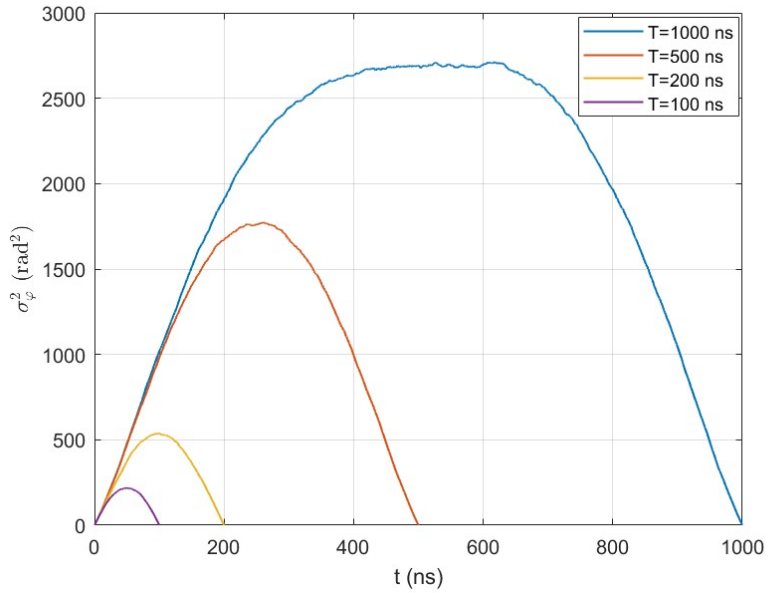


Figure 4.10: The variance $\sigma_\varphi^2$ versus time $t$ of one time interval, for $T = 1000$, 500, 200 and 100 ns.

The results in Figure 4.10 are overall significantly different for every choice of $T$. However, analysing at small times, $t << T$, it is clear that they are much closer one another. To visualise that, in Figure 4.11 the same results are plotted but only up to a time $t = 20$ns.

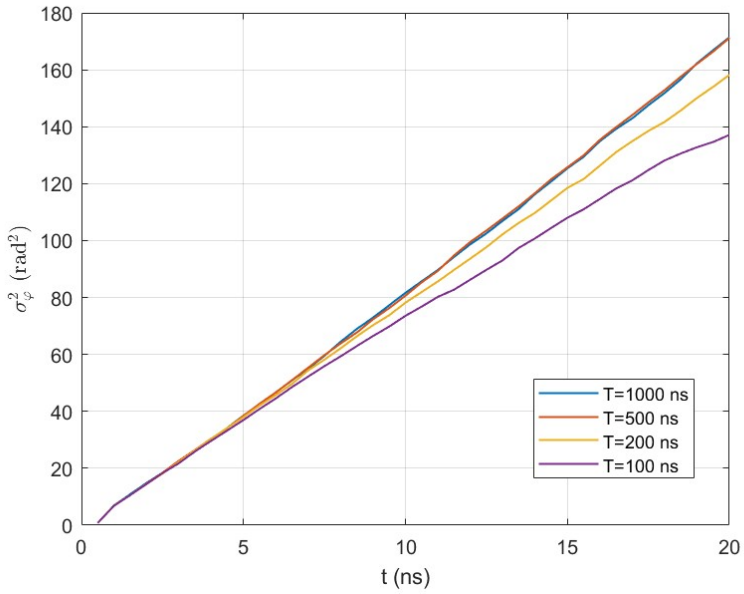


Figure 4.11: The variance $\sigma_\varphi^2$ versus time $t$ up to 20ns, for $T = 1000$, 500, 200 and 100 ns.

Now, in Figure 4.11 all variance values are very similar, and approach linear functions of time. Moreover, the $T = 500$ns variance is really close to the $T = 1000$ns variance, which shows there is a convergence to that value. Similarly to the reasoning done for Brownian motion with the reduction of $\Delta t$, this shows that the variance converges in the small time regime $t << T$. Analogously as well to what was done for Brownian motion, a normalised histogram of the number of trajectories ordered by their phase noise $\varphi$ value is plotted in Figure 4.12. This is done for a time $t = 20$ns, in the small time regime $t << T$.

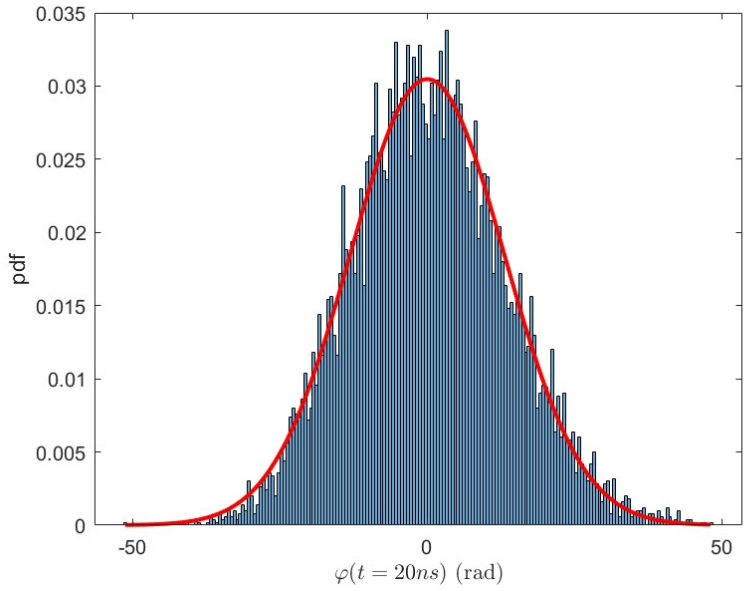


Figure 4.12: Normalised histogram of the phase noise $\varphi$ of the trajectories at a time $t = 20$ns. A red Gaussian pdf approximates the data.

The distribution of the phase noise $\varphi$ shown in the plot is very close to a Gaussian, as can be seen by plotting the Gaussian distribution corresponding to the standard deviation of the data and mean 0 in red. The diffusion of the phase noise is characterised by the diffusion coefficient, $D_\varphi$, defined by $\sigma_\varphi^2 = 2D_\varphi t$, for $t << T$. $D_\varphi$ can be obtained from a linear fit in Figure 4.11 for $t = 1000$ns. The result is $D_\varphi = 4.67 \pm 0.01$ rad$^2$/ns, with a regression coefficient of 0.99989. Keeping these results in mind, the next chapter develops on the main goal of this work, which is to understand which type of Brownian motion better describes the experimental phase noise $\varphi$ in a semiconductor laser.

# Chapter 5

# Discussion & Conclusions

In the final chapter of this work, the aim is to compare the experimental results of the phase noise $\varphi$ from Chapter 4 with the numerical results of 1D and 2D Brownian motion, developed in Chapter 3. That comparison is performed using the different statistical moments and distributions determined in both chapters, and studying their relationship with the SDEs of both Brownian motion and the semiconductor laser.

## 5.1 Discussion of the Experimental Results

### 5.1.1 Semiconductor Laser Equations and Brownian Motion

In the second chapter of this work, subsection 2.3.4, the stochastic rate equations for a semiconductor laser were introduced. Two different sets of equations were introduced. The first three equations, (2.24)-(2.26), considered the current $I$ in the laser to be constant over time, and were derived from first principles. Equation (2.25) is the one that describes the phase $\phi$ of the laser in that case:

$$\frac{d\phi}{dt} = \frac{\alpha}{2}\left[G_N(N - N_t) - \frac{1}{\tau_P}\right] + \sqrt{\frac{\beta B}{2\bar{P}}}\bar{N}F_\phi(t)$$

where $F_\phi$ is a Gaussian white noise. The evolution of $\phi$ can be well approximated by 1D Brownian motion in Eq. (2.25) when $I < I_{th}$ because the noise term (right) dominates over the deterministic term (left). This means that the distribution of $\phi$ is Gaussian, and therefore finite values of $\sigma_\phi^2$ are obtained, with a linear dependence on $t$ just like in one dimensional Brownian motion.

On the other hand, it was explained how when the current $I$ is not constant, historically the solution has been to write the same equations but changing averages over time $\bar{P}$ and $\bar{N}$ by the variables, and $I$ by $I(t)$. This approach is not based on first principles, and gives another set of three equations, (2.27)-(2.29). These are mathematically equivalent to equations (2.30) and (2.31), which use the complex electric field $E(t) = E_1 + iE_2$. The equation that describes this electric field is equation (2.30):

$$\frac{dE}{dt} = \left[\left(\frac{1}{1 + \epsilon \mid E \mid^2} + i\alpha\right) G_N(N - N_t) - \frac{1 + i\alpha}{\tau_p}\right]\frac{E}{2} + \sqrt{\frac{\beta B}{2}}N\xi(t)$$

Recall that the phase of the electric field, i.e. the argument of the complex number $E(t) = E_1 + iE_2$, was written as $\Phi$, to differentiate it from the phase $\phi$ in the first set of equations. For bias currents below threshold, $I < I_{th}$, equation (2.30) can be approximated by 2D Brownian

motion, again because the deterministic term (left) is much smaller than the noise term (right). In fact, using these last equations, it has been shown that the variance of $\Phi$ diverges $\sigma_\Phi^2 = \infty$ [17], just like it was shown here for two-dimensional Brownian motion.

### 5.1.2 Which set of equations better describes the experimental results?

It is the time to try to answer the main question in this work. Between the two, which set of equations better describes the experimental results? As explained in the previous subsection, 5.1.1, this is equivalent to comparing the statistical moments and distributions of the experimental results with those of 1D and 2D Brownian motion.

It is important to note that, in the experimental results, the optical phase noise $\varphi(t)$ was studied, which is not exactly the same as the phases $\phi$ and $\Phi$ in the semiconductor laser rate equations. It was explained in subsection 2.3.4 that, in equations (2.24)-(2.26), $\phi$ is the optical phase in the reference frame of the threshold frequency $\omega_{th}$. This means that the phase of the laser would be $\omega_{th}t + \phi(t)$. On the other hand, the phase of the laser was written in section 4.1 as $\omega_s t + \varphi(t)$. Therefore, it can be concluded that:

$$\phi(t) = (\omega_s - \omega_{th})t + \varphi(t) \tag{5.1}$$

Since $(\omega_s - \omega_{th})t$ is not a random variable, it is understood that the statistical properties of both $\phi$ and $\varphi$ will be the same. That is, $\sigma_\varphi^2 = \sigma_\phi^2$, and if $\phi$ is Gaussian, $\varphi$ is also Gaussian with a mean value different by a constant $(\omega_s - \omega_{th})t$. Moreover, $(\omega_s - \omega_{th}) << \omega_s$, and therefore both $\phi$ and $\varphi$ are almost the same. The exact same applies to the phase $\Phi$ in equations (2.27)-(2.29).

At this point, the conclusion may already seem evident. As explained several times, the results of $\theta$ and $\varphi$ from the numerical algorithm that is employed to analyse the data are only valid in the small time regime, $t << T$. For small times, it is shown that the method gives variance $\sigma_\varphi^2$ values that converge to a linear function of time, as explained in Figure 4.11. This convergence shows that the stochastic process has a finite variance, and moreover that this variance is a linear function of time.

Furthermore, it was shown in Figure 4.12 that the probability distribution of the stochastic process $\varphi$ already approaches a Gaussian for small times $t = 20$ns. These two properties, as was shown in Chapter 3, are characteristic of 1D Brownian motion. It can be thereby concluded that, the set of equations, from the two described in Chapter 2, which better describe the experimental data, are equations (2.24)-(2.26).

## 5.2 Conclusions

The main conclusion of this work is that the experimental measurement of the phase noise $\varphi$ in a semiconductor laser is a stochastic process with finite variance and Gaussian distribution. This makes it very similar to one dimensional Brownian motion, which has a Langevin equation which is like the equation for $\phi$ in (2.24)-(2.26), but without the deterministic term.

To describe $\varphi$ mathematically, studies on QRNG based on gain-switching of semiconductor lasers, have usually used equations (2.27)-(2.29), which are equivalent to equations (2.30) and (2.31) [3, 17, 22, 23, 24, 25, 26, 27] . These equations, though, are similar to the Langevin equations of 2D Brownian motion; and therefore, as shown by [17], they imply $\sigma_\Phi^2 = \infty$. Furthermore, the phase $\Phi$ of 2D Brownian motion has a Cauchy probability distribution, which is

very different from the Gaussian distribution.

These findings provide robust theoretical and experimental support for equations (2.24)-(2.26), which offer a comprehensive explanation of the results. Additionally, they cast doubt on the use of equations (2.27)-(2.29) and (2.30)-(2.31) when current is below the threshold value, which can't explain the convergence of the variance of $\varphi$ and its Gaussian distribution. Although they have been used in the latest bibliography on gain-switched semiconductor lasers for QRNG, the use of equations (2.27)-(2.29) and (2.30)-(2.31) is not considered correct, considering these results. They just give an approximation of the real results. The goal would be to find a modification of these equations that avoids the divergence of the variance and explains the Gaussian distribution of the results.

# Bibliography


[1] https://www.techtarget.com/searchsecurity/definition/cryptography Accessed: April 21, 2024.

[2] https://www.nsa.gov/Cybersecurity/Quantum-Key-Distribution-QKD-and-Quantum-Cryptography-QC/ Accessed: April 21, 2024.

[3] Paraíso Taofiq K., Woodward Robert I., Marangon Davide G. et. al. *Advanced laser technology for quantum communications (tutorial review)*, Advanced Quantum Technologies, Wiley Online Library, 2100062, (2021).

[4] Miguel Herrero-Collantes, Juan Carlos Garcia-Escartin. *Quantum Random Number Generators.* Review of Modern Physics, 89, 015004 (2017).

[5] Omar Alkhazragi, Hang Lu, Wenbo Yan et. al. *Semiconductor Emmiters in Entropy Sources for Quantum Random Number Generation* Annalen de Physik, 2300289, (2023).

[6] https://www.britannica.com/science/Brownian-motion Accessed: March 5, 2024

[7] C.W. Gardiner, *Handbook of Stochastic Methods: for Physics, Chemistry and the Natural Sciences.* (Springer-Verlag, Berlin, 1983.)

[8] Lothar Breuer, *Introduction to Stochastic Processes*, Available online: *https://www.kent.ac.uk/smsas/personal/lb209/files/notes1.pdf*, Accessed: March 5, 2024.

[9] Asloob Mudassar *Laser Physics*. 1st ed., Pakistan Institute of Engineering and Applications, (2015).

[10] F. Sanz y J.A. Manzanares *El láser de semiconductor.* Revista Mexicana de Física 37 No. 2 382-390. (1991).

[11] https://fiberguide.net/laser-diodes/

[12] S. M. Sze , *Physics of Semiconductor Devices*, John Wiley & Sons, Inc. (1981).

[13] R. Paschotta, article on "Gain Switching" in the RP Photonics Encyclopedia, retrieved 2024-04-29, https://doi.org/10.61835/va1

[14] L. A. Coldren, S. W. Corzine, M. L. Mashanovitch, *Diode Lasers and Photonic Integrated Circuits* vol 218, (John Wiley & Sons, New York, 2012)

[15] Petermann K. *Laser diode modulation and noise* vol 3 (Springer Science & Business Media, 1991)

[16] Lovic V., Marangon D. G., Lucamarini M., Yuan Z. and Shields A. J. *Physical Review Applied.* 16, 054012, (2021).

[17] A. Valle *Divergence of the Variance of the Optical Phase in Gain-Switched Semiconductor Lasers Described by Stochastic Rate Equations* Physical Review Applied 19, 054005 (2023).

[18] M. P. Lévy. *Le mouvement brownien plan.* American Journal of Mathematics 62, 487 (1940).

[19] F. Spitzer *Some theorems concerning 2-dimensional Brownian motion.* American Mathematical Society 87, 187 (1958).

[20] https://kylia.com/api-website-feature/files/download/11117/datasheet-COH-V12.pdf

[21] Kazuro Kikuchi, *Characterization of semiconductor-laser phase noise and estimation of bit-error rate performance with low-speed offline digital coherent receivers.* Opt. Exp., 20, 5292, (2012).

[22] Lovic V., Marangon Davide Giacomo, Lucamarini Marco et. al. *Characterizing Phase Noise in a Gain-Switched Laser Diode for Quantum Random-Number Generation*, Physical Review Applied, 16, 054012, (2021).

[23] Septriani Brigitta, de Vries Oliver, Steinlechner Fabian et. al. *Parametric study of the phase diffusion process in a gain-switched semiconductor laser for randomness assessment in quantum random number generator*, AIP Advances, 10, 055022, (2020).

[24] Shakhovoy Roman, Sharoglazova Violetta, Udaltsov Alexander et. al. *Influence of Chirp, Jitter, and Relaxation Oscillations on Probabilistic Properties of Laser Pulse Interference*, IEEE Journal of Quantum Electronics, 57, 1, (2021).

[25] Shakhovoy Roman, Puplauskis Marius, Sharoglazova Violetta et. al. *Phase randomness in a semiconductor laser: Issue of quantum random-number generation*, Physical Review A, (2023).

[26] Abellán Sánchez Carlos, *Quantum random number generators for industrial applications*, PhD Thesis, Universitat Politècnica de Catalunya, (2018).

[27] Quirce Ana and Valle Ángel, *Spontaneous emission rate and phase diffusion in gain-switched laser diodes*, Optics & Laser Technology, 150, 107992, (2022).

# Appendix A

`brownian-motion-1D.m` calculates $N$ trajectories of 1D Brownian motion:

```
function [X] = brownian_motion_1D(x0, t_i, t_f, D, delta_t, DELTA_T, N)
% Input:
%   x0          - Initial condition of the Brownian motion.
%   t_i         - Initial time.
%   t_f         - Final time.
%   D           - Diffusion coefficient.
%   delta_t     - Calculation time step.
%   DELTA_T     - Writing time step.
%   N           - Number of independent trajectories.
%
% Output:
%   X           - Matrix containing N rows (trajectories) and no_intervals
%                 columns (times)
if t_i>=t_f
    fprintf('Error: t_i>=t_f')
    return
end
no_intervals = round((t_f-t_i)/DELTA_T); %writting time intervals
no_subintervals = round(DELTA_T/delta_t); %calculation times subintervals
X = zeros(N,no_intervals); %exit variable
for i = 1:N %N independent trajectories
    x = x0; %start with the initial condition
    for j = 1:(no_intervals) %run writting intervals
        for k = 1:no_subintervals %run calculation intervals
            x = x + sqrt(2*D*delta_t)*normrnd(0,1);
        end
        X(i,j) = x;
    end
end
end
```

# Appendix B

`brownian-motion-2D.m` calculates $N$ trajectories of 2D Brownian motion, and their respective phase $\Phi$, using the function `calculate-phase.m`:

```
function [X1,X2,phase] = brownian_motion_2D(x0, y0, t_i, t_f, D, ...
                                                    delta_t, DELTA_T, N)
% Input:
%   x0          - Initial x condition of the Brownian motion.
%   y0          - Initial y condition of the Brownian motion.
%   t_i         - Initial time.
%   t_f         - Final time.
%   D           - Diffusion coefficient.
%   delta_t     - Calculation time step.
%   DELTA_T     - Writing time step.
%   N           - Number of independent trajectories.
%
% Output:
%   [X1, X2]      - Array containing 2 matrices (x,y), N rows (trajectories)
%                   and no_intervals columns (times)
%
%   phase         - Array containing the phase, N rows (trajectories) and
%                   no_intervals columns (times)
if t_i>=t_f
    fprintf('Error: t_i>=t_f')
    return
end
m=0; %nof clockwise crossings
n=0; %nof counterclockwise crossings
no_intervals = round((t_f-t_i)/DELTA_T); %writting time intervals
no_subintervals = round(DELTA_T/delta_t); %calculation times subintervals
X1 = zeros(N,no_intervals); %exit variables
X2 = zeros(N,no_intervals);
phase  = zeros(N,no_intervals);
```

```
for i = 1:N %N independent trajectories
    x = x0; %start with the initial conditions
    y = y0;
    X1(i,1) = x0;
    X2(i,1) = y0;
    %FIRST MOVEMENT
    x = x + sqrt(2*D*delta_t)*normrnd(0,1);
    x_ini = x;
    y = y + sqrt(2*D*delta_t)*normrnd(0,1);
    y_ini = y;
    %ALL NEXT MOTION
    for j = 2:(no_intervals) %run writting intervals
        for k = 1:no_subintervals %run calculation intervals
            x_new = x + sqrt(2*D*delta_t)*normrnd(0,1);
            y_new = y + sqrt(2*D*delta_t)*normrnd(0,1);
            [phi, n_new, m_new] = calculate_phase(x,y,x_new,y_new,m,n, ...
                                                                x_ini,y_ini);
            n = n_new;
            m = m_new;
            x = x_new;
            y = y_new;
        end
        X1(i,j) = x;
        X2(i,j) = y;
        phase(i,j) = phi;
    end
    n=0; %restart n and m
    m=0;
end
end
```

```
function [phi, n_new, m_new] = calculate_phase(x,y,xn,yn,m,n,x_ini,y_ini)
t1x = x*xn;
t2x = y*x;
if x_ini >= 0 %Q1 or Q4
    if t1x < 0 %cross vertical axis
        if t2x >= 0 %point in Q1
            n_new = n+1; %counterclockwise
            m_new = m;
            if x>0 && yn<0 %Q1 --> Q3
                if normrnd(0,1)>0
                    n_new = n_new -1;
                    m_new = m_new +1;
                end
            end
            if x<0 && yn>0 %Q3 --> Q1
                if normrnd(0,1)>0
                    n_new = n_new -1;
                    m_new = m_new +1;
                end
            end
        else %point in Q2 or Q4 --> Q4
            n_new = n;
            m_new = m+1; %clockwise
            if x<0 && yn<0 %Q2 --> Q4
                if normrnd(0,1)>0
                    n_new = n_new +1;
                    m_new = m_new -1;
                end
            end
```

```
            if x>0 && yn>0 %Q4 --> Q2
                if normrnd(0,1)>0
                    n_new = n_new +1;
                    m_new = m_new -1;
                end
            end
        end
    else % t1x >= 0 --> doesn't cross axis
        n_new = n;
        m_new = m;
    end
    phi = atan(yn/xn) + (n_new-m_new)*pi;
else %x_ini < 0
    if y_ini < 0 %Q3 --> atan>0 --> -pi
        param = -1;
    else %y_ini > 0 %Q2 --> atan<0 --> +pi
        param = +1;
    end
    if t1x < 0 %cross vertical axis
        if t2x >= 0 %point in Q1 or Q3
            n_new = n+1; %counterclockwise
            m_new = m;
            if x>0 && yn<0 %Q1 --> Q3
                if normrnd(0,1)>0
                    n_new = n_new -1;
                    m_new = m_new +1;
                end
            end
```

```
            if x<0 && yn>0 %Q3 --> Q1
                if normrnd(0,1)>0
                    n_new = n_new -1;
                    m_new = m_new +1;
                end
            end
        else %point in Q2 or Q4
            n_new = n;
            m_new = m+1; %clockwise
            if x<0 && yn<0 %Q2 --> Q4
                if normrnd(0,1)>0
                    n_new = n_new +1;
                    m_new = m_new -1;
                end
            end
            if x>0 && yn>0 %Q4 --> Q2
                if normrnd(0,1)>0
                    n_new = n_new +1;
                    m_new = m_new -1;
                end
            end
        end
    else % t1x >= 0
        n_new = n;
        m_new = m;
    end
    phi = atan(yn/xn)+(n_new-m_new+param)*pi; %param to correct atan
end
% Modified by Iker Pascual de Zulueta from the work of Ángel Valle.
end
```

# Appendix C

`experiment.m` calculates the phases $\theta$ and $\varphi$ of $N$ trajectories from the file *'data'*, using the function `calculate-phase.m`:

```
function [X1,X2,theta_list,phase,domega_list,times] = experiment(data, N)
% Input:
%   data       - 3 column data: times, E1 and E2
%   N          - Number of independent trajectories.
%
% Output:
%   X1         - N x ip array, E1.
%   X2         - N x ip array, E2.
%   theta_list - N x ip array, phase theta between E1,E2.
%   phase      - N x ip array, varphi.
%   domega_list- 1 x N array, Delta omega
%   times      - 1 x ip array, times, t=0 to t=ip*500e-12

fid = fopen(data, 'r'); %read data
fileData = textscan(fid, '%f %f %f', 'Delimiter', '\t');
fclose(fid);
times_tot = fileData{1};
X1_tot = fileData{2};
X2_tot = fileData{3};

ifich  = 20000000;  %number of total data points
ip     = ifich/N;  %points in every trajectory
delta_t = 500e-12;

N=10000; %limit to N=10000
X1 = zeros(N,ip); %initiate exit variables
X2 = zeros(N,ip);
phase = zeros(N,ip);
times = zeros(1,ip); %list of times t1=0, tip=T
theta_list  = zeros(N,ip);
domega_list = zeros(1,N);
```

```
for j = 1:ip
    times(j) = j*delta_t;
end
m=0; %nof clockwise crossings
n=0; %nof counterclockwise crossings
for i = 1:N %N independent trajectories
    sumder = 0; %sum of d\theta/dt
    fprintf('i=%d\n', i);
    x_ini  = X1_tot((i-1)*ip+1); %start with the initial conditions
    y_ini  = X2_tot((i-1)*ip+1);
    X1(i,1) = x_ini;
    X2(i,1) = y_ini;
    x = x_ini;
    y = y_ini;
    theta = atan(y_ini/x_ini);
    theta_list(i,1) = theta; %calculate theta(0)!=0
```

```
    %ALL NEXT MOTION
    for j = 2:(ip) %run writting intervals
        x_new = X1_tot((i-1)*ip+j);
        y_new = X2_tot((i-1)*ip+j);
        [theta_n, n_new, m_new] = calculate_phase(x,y,x_new,y_new,m,n, ...
                                                  x_ini,y_ini);
        % [x_new,y_new,phi,n_new,m_new]
        % pause
        n = n_new;
        m = m_new;
        x = x_new;
        y = y_new;
        X1(i,j) = x;
        X2(i,j) = y;
        sumder = sumder + (theta_n-theta)/delta_t;
        theta = theta_n;
        theta_list(i,j) = theta;
    end
    %restart n and m
    domega = sumder/(ip-1);
    phase(i,:) = theta_list(i,:) - domega*times;
    domega_list(i) = domega;
    n=0;
    m=0;
end
end
```